TOPOLOGICAL REALIZATIONS OF ENTANGLING QUANTUM GATES

THESIS

Adrian D. Scheppe, 2Lt, USAF

AFIT-ENP-MS-21-M-134

DEPARTMENT OF THE AIR FORCE
AIR UNIVERSITY

AIR FORCE INSTITUTE OF TECHNOLOGY

Wright-Patterson Air Force Base, Ohio

AFIT-ENP-MS-21-M-134

Topological Realizations of Entangling Quantum Gates

THESIS

Presented to the Faculty

Department of Applied Physics

Graduate School of Engineering and Management

Air Force Institute of Technology

Air University

Air Education and Training Command

in Partial Fulfillment of the Requirements for the

Degree of Master of Science in Applied Physics

Adrian D. Scheppe, B.S.

2Lt, USAF

March 25, 2021

AFIT-ENP-MS-21-M-134

Topological Realizations of Entangling Quantum Gates

THESIS

Adrian D. Scheppe, B.S.
2Lt, USAF

Committee Membership:

Mike M Pak, Ph.D
Chair

David M Weeks, Ph.D
Member

Anil Patnaik, Ph.D
Member

Larry Merkle, Ph.D
Member

AFIT-ENP-MS-21-M-134

Abstract

Quantum information science and quantum computing are currently plagued by decoherence, a naturally occurring process which stems from quantum fluctuations and the environment's natural tendency for entropy to increase. This process causes information loss and presents severe difficulties for current multi qubit systems. Topological systems are immune to such fluctuations and provide a hunting ground for qubits that are fault tolerant. Majorana fermions within 2D $p_x + ip_y$ wave topological superconductors are a particular realization of a topologically protected qubit which has gained much attention because of the possible ease and speed of manipulation. The process of calculating linear operator representations of Majorana fermion exchanges or braids is well known and well documented; however, there is no documented intuition or algorithm which provides the opposite; braids from quantum gates. In this document, all possible linear representations of single, double, triple, and quadruple qubit gates are calculated to find several key patterns which provide crucial insight into the manifestation of qubit gates. A $n \times n$ gate will require $n+2$ Majoranas with $\frac{1}{2}n+1$ trivial braids and $\frac{1}{2}n$ coupling braids possible. The native gates produced are either tensor products or tensor sums of the well known phase gate and Pauli $\mathbf{X}$ gate, demonstrating that a topological SC Majorana qubit may only explore the poles of the Bloch sphere. Additionally, the exact compact forms of all possible gates are listed. These insights are an important step to the formation of a complete understanding of the braids' effects on the multi qubit system which is necessary if one is to take advantage of this fault tolerant method of quantum computation. It is hopeful that in future works, an exact algorithm for determining the braid representation of a quantum gate will be delineated.

Table of Contents

List of Figures

Figure Page

I. Introduction

Google's 2019 publication titled "Quantum supremacy using a programmable superconducting processor" [1] punctuated over fifty years of theories, discoveries, and breakthroughs, and it posed the exciting possibility of finally reaching one of this century's greatest milestones, a programmable quantum computer. The creation of such a device with the processing power of a regular laptop computer would be on the same order of magnitude of importance as manned space flight or nuclear energy. However, the state of the art systems at Google, IBM, Baidu, and Alibaba share the common problem of decoherence stemming from the ever present quantum fluctuations of the environment. In terms of von Neumann entropy and information theory, the pure computational states couple with the environment which results in all off-diagonal terms becoming zero in the qubit environment mixed density matrix. The natural pure to mixed state transition is a result of entropy increase, destroys the quantum state, and results in information losses [2]. Clearly, in the setting of quantum computation, one would hope to minimize these losses hence the large effort in the subfield of error correction, but, even with corrections, decoherence is a massive hurdle to the scaling of quantum computers. On the surface, it would seem that local perturbations are an evil that will forever haunt quantum information. However, there does exist a class of systems with Hamiltonians and associated eigenstates that are topological in nature and are immune to such perturbations.

These so called topological states of matter are condensed matter systems equipped with a degenerate ground state manifold that is separated from the remaining spec-

trum via an energy gap. By forming a computational basis from the ground state manifold, it is feasible to construct a quantum computer with states which do not couple via local perturbations. Such a computer would be fault tolerant or decoherence proof [2].

There are copious examples of well studied systems with varying flavors and temperaments that exhibit this quality. A promising candidate and the subject of this work makes use of Majorana fermions in 2D p_x+ip_y wave superconductors (SC). These exotic quasi particles emerge where the SC gap closes within Abrikosov vortices or on the physical boundaries of the system. They are zero energy mode excitations that annihilate themselves, or, equivalently, its Fock space creation operator is hermitian. Due to the 2D nature of the system, Majorana exchange statistics may be qualitatively different than 3D particle statistics. In three dimensions, indistinguishable particles exchange symmetrically (Bosons) or antisymmetrically (Fermions); however, 2D particles may exchange with any phase change in between 0 and π obeying anyonic statistics instead. Rephrasing using group theory terminology, the finite permutation group, P_n, describes Abelian n-fermionic or bosonic exchange statistics. The exchanges that n Majorana fermions may make are characterized by the non-Abelian infinite braid group, B_n, where only equivalence classes of braids have linear representations that rotate the ground state manifold. Therefore, by forming a computational basis from the members of this manifold, Majorana braids generate transformations of the computational states.

The methods which outline direct calculation of a unitary operator from a braid are well documented; however, it is still uncertain the method by which one may calculate the opposite: quantum gates to braids. The opposite direction of calculation is crucial to constructing an accessible quantum computer. Quantum computation and quantum information science is a diverse field with mathematicians, computer

scientists, and physicists, and, for this reason, a large portion of research in this field is somewhat unconcerned with the physical realization of a qubit. Instead, much of this research is performed with no particular qubit in mind, where the literature only mentions quantum gates, states $|0\rangle$ and $|1\rangle$, and circuit diagrams. This fact serves as motivation for the delineation and characterization of quantum gate realizations of Majorana braids.

In this work, there will be sections dedicated to topics introduced above with a particular focus on topological protection, Majorana fermions, and braid groups. Then, all possible linear representations of braids will be calculated for the two, four, six, and eight Majorana cases. Following direct calculation, there will be a discussion section dedicated to developing intuitions and cataloging the affects of braids on the multi-qubit system. Finally, using these rules and intuitions, the beginnings of an algorithm will be formed.

II. Background and Literature Review

2.1 Topological Protection

In 2008, Divincenzio provided a short list of criteria that the ideal qubit should have [3]:

i. *Simple Fiducial State Initialization*

ii. *Single Qubit Measurement*

iii. *Sufficiently Long Decoherence Times*

iv. *Scalability*

v. *Universal Quantum Gates*

Without a doubt, the criterion that poses the largest threat to quantum computing in recent years has been criterion iii. Many natural and engineered quantum systems have been proposed for a qubit; however, they are all affected by decoherence because a system left to evolve on its own will increase in entropy. In a quantum system, von Neumann entropy encodes the system's departure from a pure state, meaning the fiducial states established for a particular qubit will naturally couple to the state of the environment [4]. Once a measurement is taken, the total state collapses resulting in information loss. Furthermore, conventional gate operations for these systems are implemented via some local interaction potential. The energy exchange during this interaction causes additional noise and is the source of the imprecision in current quantum gates [5].

Currently, decoherence is managed through error correction methods and attempted environmental separation, but these techniques will never completely fix the problem. Error correction only addresses the pure state transition, e.g. $|0\rangle \rightarrow$

$\alpha |0\rangle + \beta |1\rangle$ which is a consequence of using an approximate Hamiltonian to describe the system instead of the unknowable exact Hamiltonian. These methods assume that the original state is recoverable through some unitary transformation, and they do not address the mixed state transition stemming from the environmental fluctuations.

In an effort to locate a solution, one may start over and form a wish list of qubit qualities. A well known virtue of quantum mechanics is that not all energy eigenstates are affected by decoherence uniformly. Higher energy states decohere faster and more dramatically than lower energy states [6]. Thus, the establishment of computational states from a degenerate ground state would minimize the environmental affects. Additionally, $|0\rangle$ and $|1\rangle$ within this ground state should themselves be immune to the noisy environment with no available process of coupling through local means. Rather, it would be preferable if the qubits coupled through *global* symmetries [5]. As shown by Kitaev, these three qualities are realized and may be implemented by topological phases of matter [7].

Classically, phases of matter may be categorized by using a broken symmetry or an order parameter, which quantifies the degree in which the system resides in a particular phase [8]. For example, fluid water transitioning to solid would exhibit a broken rotational symmetry as depicted in Figure 1. The ice no longer possesses continuous rotational and translational symmetry like the fluid. Instead, the lattice must slide left, right, or rotate by discrete amounts to appear symmetric. In contrast to this method of categorization, 20th century researchers discovered that several emergent phases of matter did not correspond with any broken symmetries [9]. Figure 2 lists several states such as Integer and Fractional Quantum Hall states, spin liquids, and topological insulators as examples [10]. It is now apparent that these systems exhibit long range entanglement and are topologically ordered. Each system in Figure 2 has an associated topologically invariant parameter which may be used as classification

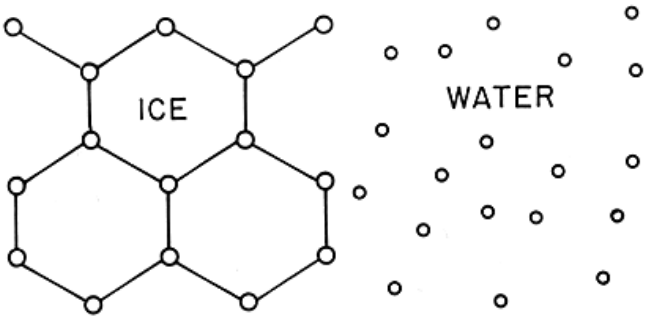

Figure 1: Rotational Symmetry of Ice [8]. Liquid water is rotationally and translationally invariant; however, ice is only symmetric to discrete shifts and turns. As the state transitions from one to the other, symmetry is said to be broken.

tool [11][12][13].

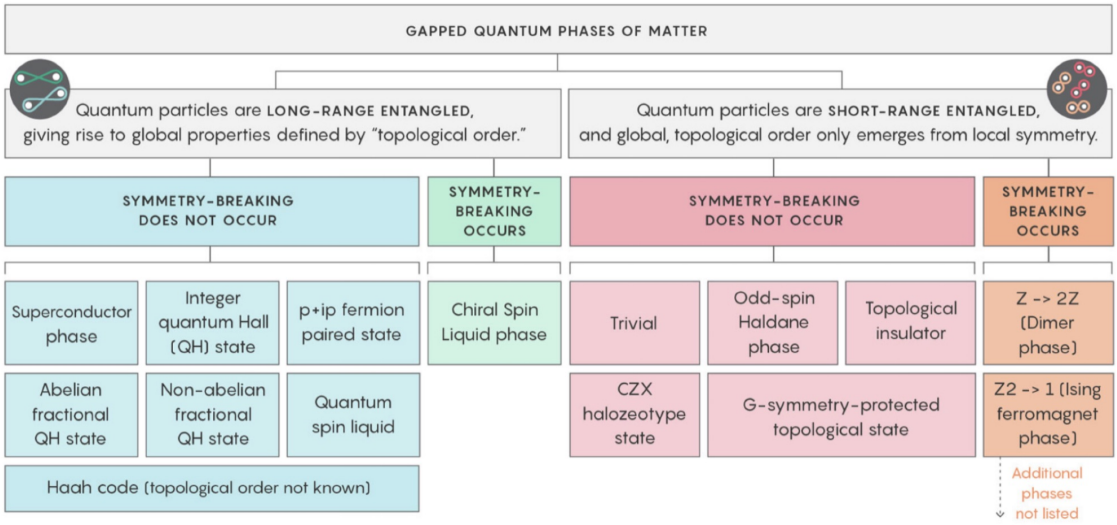

Figure 2: Gapped Quantum Phases of Matter [10].

To better demonstrate the concepts presented above, an example of an abstract qubit formed from one of these states may be helpful [9]. There exists a 2D topological phase of matter named Spin Liquid which is shown on the left of Figure 3. This system exhibits long ranged entanglement in the form of long strings of identical spin particles. The liquid is subjected to constant perturbations from the environment, and, as a result, the chains of entangled particles are in constant flux moving about

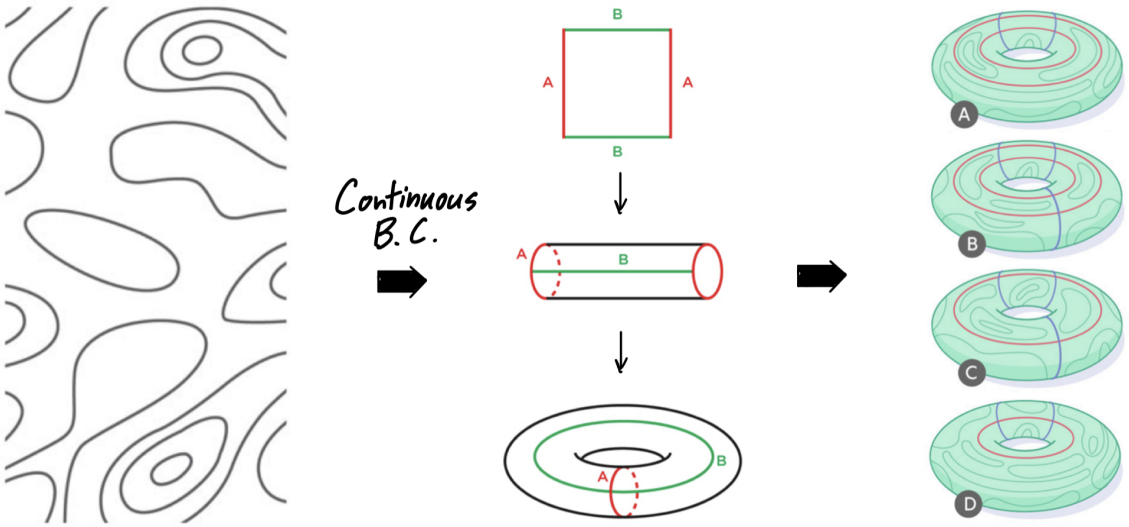

Figure 3: Topologically Ordered Spin Liquid [10]. The 2D spin liquid is a topologically ordered state of matter. To reveal the underlying topological invariance, one applies continuous boundary conditions by connecting the parallel borders of the left most image. This process maps the 2D plane to a torus, where the topological invariant parameter manifests as the even or odd number of connected loops that encircle the hole and go through the hole. This splits the ground state of this system into four possible equivalence classes, $|A\rangle$, $|B\rangle$, $|C\rangle$, and $|D\rangle$.

the 2D system erratically. To expose the topological order of this phase, one simply imposes continuous boundary conditions. That is, the parallel borders of the left hand image in Figure 3 are brought together to meet one another, basically mapping the two dimensional plane to the surface of a torus. Topological invariance manifests as the even or odd number of the strings wrapping through and around the hole. This splits the system's ground state into four equivalence classes depicted on the right most image in Figure 3: $|A\rangle$ (even-even), $|B\rangle$ (even-odd), $|C\rangle$ (odd-odd), or $|D\rangle$ (odd-even). As the system is perturbed, strings will combine and break apart; however, the parity of the system will remain invariant to these perturbations. In other words, if this ground state manifold were hypothetically used as a computational space, state $|A\rangle$ would *never* decohere to state $|B\rangle$ without some global interaction. This This example demonstrates the essence of topological protection.

2.2 Quick Review of Superconductivity

The Majorana discussed in this work are emergent quasiparticle excitations from the SC state. In an effort to give the reader context for these excitations, a quick review of the SC state is provided here. This material comes from various SC and quantum field theory reviews [14][15][16].

Following London's theoretical description of the experimental phenomena of the SC state, Ginzberg-Landau form another set of equations which come from thermodynamical arguments and minimization of the free energy functional,

$$\frac{1}{4m}(-i\hbar\nabla - 2e\mathbf{A})^2\Psi - \alpha|t|\Psi + \beta|\Psi|^2\Psi = 0 \tag{1}$$

$$\mathbf{n}\cdot(-i\hbar\nabla + 2e\mathbf{A})\Psi = i\frac{\Psi}{b}. \tag{2}$$

Equation 1 minimizes the aforementioned free energy functional and describes the behavior of the SC state within a material. Equation 2 is the boundary condition of the SC order parameter, Ψ, at the interface of the SC and normal regions. These equations allow physicists to form descriptions of the behavior of the state itself at and beyond the phase boundary.

Fundamentally, there are two different limits characterized by the ratio of London penetration depth to coherence length, $\kappa = \frac{\lambda}{\xi} \ll 1$ and $\kappa = \frac{\lambda}{\xi} \gg 1$, corresponding to type I and type II superconductors respectively. In the case of Majorana fermions, type II superconductors are the only type of interest. The small coherence length in these materials results in the induction of SC order parameter across the phase boundary into non-SC materials. In Figure 4, this property is depicted as the normalized order parameter, ψ, remaining unity across the phase boundary at the origin. Behavior such as this allows the material to enter into a mixed state which exists in between two critical magnetic field values, B_{c1} and B_{c2} and below T_c. While in

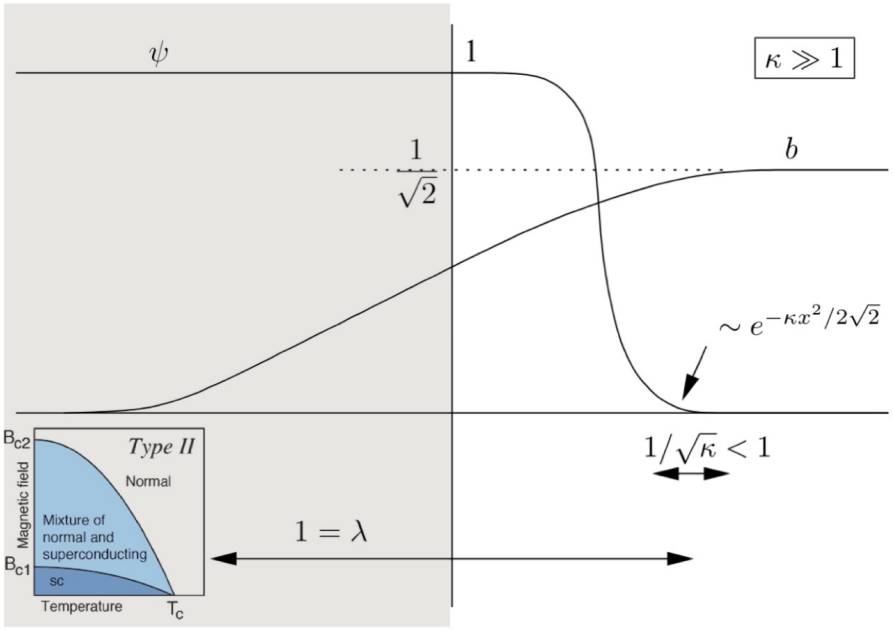

Figure 4: Type II Superconductor [14]. Depiction of an interface between SC (grey) and normal (white) region. λ and ξ are the London penetration depth and coherence length respectively, and κ is the ratio of the two. The normalized order parameter, ψ, remains unity even across the phase boundary meaning there exists an induced SC state in a normal material. This type of SC permits a mixed state which lies below T_C, and between critical magnetic fields B_{c2} and B_{c1}, and permits stable, locally normal state regions.

this mixed state, the superconductor permits the local destruction of the SC order parameter which may host exotic quasiparticle excitations.

Bardeen-Cooper-Schrieffer (BCS) theory provides a microscopic description of the SC state, which states that the fermion stack picture of regular condensed matter is unstable in a superconductor below the T_c. Instead, the new ground state is that of entangled electrons that experience a potential, Δ, from the bulk phonon interaction within the material. These cooper pairs join with opposite linear and angular momentum in an effort to minimize the total momentum.

Additionally, this new ground state experiences excitations differently than normal metals. As depicted in Figure 5, if one electron is excited from the bulk, the remaining electron may not exist alone. Instead, it is annihilated since it may not exist singularly.

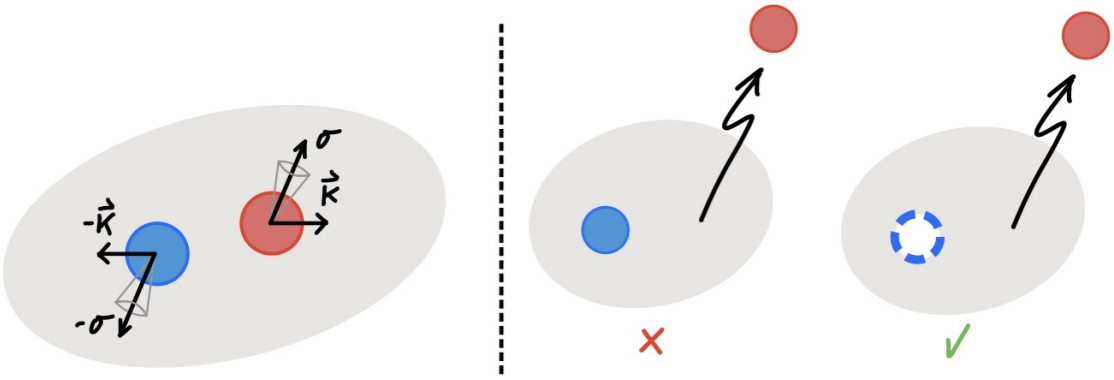

Figure 5: Bogolon Ansatz. Since the fermion stack picture is no longer stable in the condensate, the system spontaneously forms electron pairs in an effort to reach zero angular and linear momentum. Electrons cannot exist singularly in the superconductor, so, when one electron is excited, the other must be annihilated. This idea serves as a motivation for the ansatz depicted in this image.

This line of logic motivates the ansatz,

$$b_{\mathbf{k}\uparrow} = u_k c_{\mathbf{k}\uparrow} - v_k c^\dagger_{-\mathbf{k}\downarrow}$$

$$b_{\mathbf{k}\downarrow} = u_k c_{\mathbf{k}\downarrow} + v_k c^\dagger_{-\mathbf{k}\uparrow},$$

which is simply a Bogoliubov transformation of quasi electron creation and annihilation operators. These so called *bogolons* are not Majorana fermions as they are currently, i.e. $b^\dagger \neq b$. However, these math statements do provide hints as to where a Majorana may be realized. That is, the operators become hermitian when the system has one active spin species and when $u_k = v_k$. The first condition is satisfied in 1D p-wave and 2D $p_x + ip_y$-wave SC. Additionally, depicted in Figure 6, u_k and v_k are equal at the fermi level, so, as one approaches the fermi surface, $\mathbf{k} \to -\mathbf{k}$, and the bogolon creation of quasi hole and electron becomes hermitian, $b^\dagger = b$. These quasiparticle excitations are exactly the Majorana fermions discussed in this work.

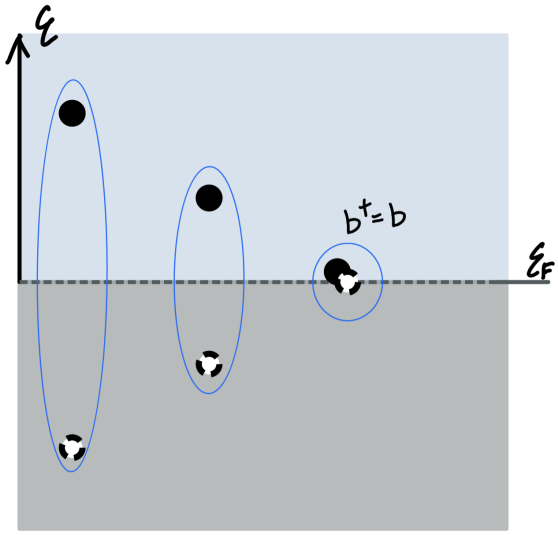

Figure 6: Majorana Fermion. Bogolons formed by combining a partial fermionic creation and annihilation operator become ambiguously defined at the fermi level. The quasi hole and electron are made on top of one another at the fermi surface, where $b^\dagger = b$.

2.3 Kitaev's Chain: Toy Model

This section is meant to be a tractable example demonstrating how Majoranas manifest and their key properties. The material here is drawn from several Majorana fermion reviews [17][18][19][5].

Depicted in Figure 7 is a 1D spinless, p-wave superconductor with N sites which can be occupied by a quasi electron. The Hamiltonian for such a system is a modifi-

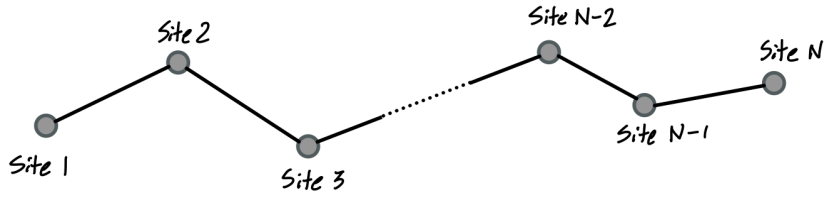

Figure 7: Kitaev's 1D, p-wave Superconductor. Each site on the chain may have one quasielectron or none.

cation of the well-known tight binding model from conduction theory,

$$\mathcal{H} = \sum_{x=1}^{N} \left[-\mu c_x^\dagger c_x - \frac{t}{2} c_{x+1}^\dagger c_n - \frac{t}{2} c_x^\dagger c_{x+1} - \frac{1}{2}\Delta e^{i\phi} c_x c_{x+1} - \frac{1}{2}\Delta e^{-i\phi} c_{x+1}^\dagger c_x^\dagger \right].$$

where, $c_x^\dagger$ and c_x will create quasi electrons and quasi holes at site x respectively. The parameter t is known as the hopping strength which is a one dimensional kinetic energy term representing the energy required to move an electron one site over if the adjacent site is unfilled. The parameter μ is the chemical potential which becomes the fermi energy as the temperature approaches absolute zero, $\lim_{T\to 0} \mu(T) = \epsilon_F$. This term is the energy a particle requires in order to populate any of the sites. As stated in Section 2.2, the fermion stack picture in a normal metal ground state is no longer a stable configuration in the SC state, so bogolons are now the natural excitations of this system. Therefore, one must include some electron-electron and hole-hole pairing terms proportional to the order parameter, Δ, with the inclusion of some arbitrary phase, ϕ. The minus signs and factors of $\frac{1}{2}$ are meant to make the following math look more pleasing.

To reveal the topological nature of this system, continuous boundary conditions will be imposed, meaning the system is wrapped into a circle by setting $c_1 = c_{N+1}$. From here, the Hamiltonian is transferred into momentum space by rewriting c_x in terms of c_k operators via a discrete fourier transform,

$$FT(c_x) \Longrightarrow \frac{1}{\sqrt{N}} \sum_k e^{-ikx} c_k.$$

Thereby transforming $\mathcal{H}$,

$$\mathcal{H} = \sum_k \left[\epsilon_k c_k^\dagger c_k - \epsilon_k c_{-k} c_{-k}^\dagger + \Delta_k c_{-k} c_k + \Delta_k^* c_k^\dagger c_{-k}^\dagger \right],$$

where $\Delta_k = i\Delta e^{i\phi}\sin(k)$ and $\epsilon_k = -\mu - t\cos(k)$. The direct calculation may be found in Appendix A.

Recognizing that the Fock space state vector is a column vector with two levels, one corresponding to negative momentum and another to positive. It is possible to block diagonalize this Hamiltonian by rearranging the indices, placing states together with odd parity,

$$\mathcal{H} = \begin{pmatrix} c_1 \\ c_{-1}^\dagger \\ c_2 \\ c_{-2}^\dagger \\ c_3 \\ c_{-3}^\dagger \\ \vdots \end{pmatrix}^\dagger \begin{pmatrix} \epsilon_1 & \Delta_1^* & & & & & \dots \\ \Delta_1 & -\epsilon_1 & & & & & \dots \\ & & \epsilon_2 & \Delta_2^* & & & \dots \\ & & \Delta_2 & -\epsilon_2 & & & \dots \\ & & & & \epsilon_3 & \Delta_3^* & \dots \\ & & & & \Delta_3 & -\epsilon_3 & \dots \\ \vdots & \vdots & \vdots & \vdots & \vdots & \vdots & \ddots \end{pmatrix} \begin{pmatrix} c_1 \\ c_{-1}^\dagger \\ c_2 \\ c_{-2}^\dagger \\ c_3 \\ c_{-3}^\dagger \\ \vdots \end{pmatrix}.$$

This reveals the motivation behind introducing the Bogoliubov-de Gennes operator, $C_k^\dagger = [c_k^\dagger, c_{-k}]$, which groups the creation of a particle and a hole together into one vector. Using this operator, one may further condense the Hamiltonian in a compact form,

$$\mathcal{H} = \sum_k C_k^\dagger \begin{pmatrix} \epsilon_k & \Delta_k^* \\ \Delta_k & -\epsilon_k \end{pmatrix} C_k. \tag{3}$$

The matrix in Equation 3 may be factored into a linear combination of Pauli spin matrices,

$$\begin{pmatrix} \epsilon_k & \Delta_k^* \\ \Delta_k & -\epsilon_k \end{pmatrix} = \epsilon_k \begin{pmatrix} 1 & 0 \\ 0 & -1 \end{pmatrix} + \Delta\sin(k)\sin(\phi) \begin{pmatrix} 0 & 1 \\ 1 & 0 \end{pmatrix} - \Delta\sin(k)\cos(\phi) \begin{pmatrix} 0 & -i \\ i & 0 \end{pmatrix},$$

and, after defining vector $\mathbf{h}$, such that $\mathbf{h} \cdot \sigma = h_x\sigma_x + h_y\sigma_y + h_z\sigma_z$, one may now parameterize every Hamiltonian through this abstract vector in a 3D parameter space. Depicted in Figure 8, as k varies throughout the Brillouin zone, a path is traced out in this space with every possible trajectory representing a different Hamiltonian parametrized by Δ, μ, t, and ϕ. The values of h_x and h_y are exactly opposite from one another and do not carry the topological information. However, $h_z = -\mu - t\cos(k)$ has the possibility of being totally negative, totally positive, or switching signs depending on where μ is located with respect to the energy band. For this reason, these trajectories split into two distinct classes:

i. *Trivial Topology ($\mu > |t|$): Blue vector trajectories that form a closed loop*

ii. *Nontrivial Topology ($\mu < |t|$): Red vector trajectories that do not form a closed loop*

The latter case will only occur if the chemical potential is located somewhere within the band while the former case occurs if it is somewhere above or below the band.

With the topology of this system in mind, set $\mu = 0$ so that the Hamiltonian is in the topologically nontrivial phase. Removing continuous boundary conditions and transitioning back to the original spatial Hamiltonian, the quasi electron operators will now be defined as an arbitrary sum of real and imaginary components,

$$c_x = \frac{1}{2}(\xi_{x,1} + i\xi_{x,2})$$
$$c_x^\dagger = \frac{1}{2}(\xi_{x,1} - i\xi_{x,2}).$$

Depicted in Figure 10, where ξ pairs are found at each site, this action is completely mathematical and has no physical meaning yet. Solving for ξ in terms of c_x and $c_x^\dagger$

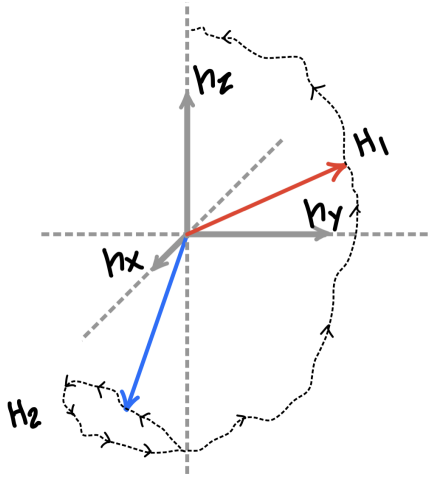

Figure 8: Topology of Kitaev's Chain. The blue arrow traces out closed loops and represents the trivial topology formed when the chemical potential, μ, lies somewhere above or below the energy band. These loops do not cross the h_x-h_y plane, but they may start and end at either pole. The red arrow represents the nontrivial topology where μ lies within the energy band which causes the h_z component of the vector to switch signs as k is varied throughout the Brillouin zone. This vector traces out a path that starts at one pole and ends on another.

and setting $t = \Delta$ and $\phi = 0$ for simplicity, one may rewrite the Hamiltonian,

$$\mathcal{H} = -\frac{t}{2}\sum_{x=1}^{N}\left[c_{x+1}^{\dagger}c_n + c_x^{\dagger}c_{x+1} + c_x c_{x+1} + c_{x+1}^{\dagger}c_x^{\dagger}\right],$$

as,

$$\mathcal{H} = -\frac{it}{2}\sum_{x=1}^{N-1}\left[\xi_{x,1}\xi_{x+1,2}\right],$$

see Appendix B for math. Since the definition of fermionic operators above was arbitrary, it is possible to form a new combination,

$$\tilde{c}_x = \frac{1}{2}(\xi_{x+1,1} + i\xi_{x,2}),$$

which may be viewed pictorially in Figure 10. This new definition simply slides the nonlocal fermion over one site. One may rewrite the Hamiltonian yet again in terms

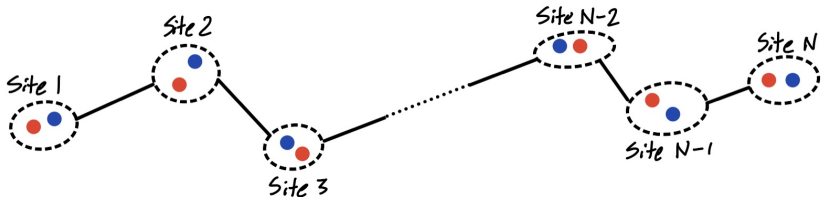

Figure 9: Kitaev Model with Majorana. The redefinition of c_x operators is completely arbitrary at this step. These operators are simply being split into real and imaginary components.

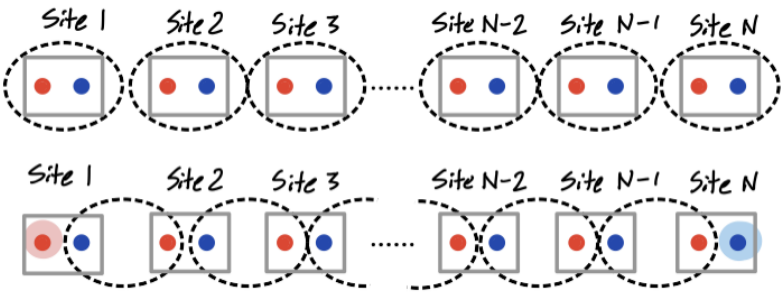

Figure 10: Redefinition of Operators. The creation operators are now redefined, grouping adjacent site ξ. This conveniently leaves the edges modes out of the final Hamiltonian meaning they correspond to the zero energy modes of the system. Since these modes are at the ground, the previously arbitrary ξ operators are now real Majorana modes that have been combined in one highly nonlocal fermion.

of these new operators,

$$\mathcal{H} = t \sum_{x=1}^{N-1} \tilde{c}_x^\dagger \tilde{c}_x,$$

where the new creation operators have diagonalized the topologically nontrivial Hamiltonian. However, the edge modes, $\xi_{N,2}$ and $\xi_{1,1}$, are completely absent from this Hamiltonian. Grouping these modes under one fermionic operator reveals that they correspond to a highly *nonlocal*, *zero energy* excitation of the topological SC state.

The edge modes written in terms of $\tilde{c}$ are exactly the same ambiguous bogolon mentioned at the end of Section 2.2 where $\gamma_2 \equiv \xi_{N,2}$ and $\gamma_1 \equiv \xi_{1,1}$ which is common in the literature. Because of the location of the excitations, these are not just math-

ematical constructs like the ξ operators, and they now correspond to the physically real Majorana zero energy modes.

This model demonstrates the following,

i. *Majorana appear at topological boundaries of the system*

ii. *Two Majoranas group to form a highly nonlocal quasiparticle*

An important clarification must be made in regards to property i. The topological boundary may not be located on the physical edge of the system. Instead, it is located on the topological boundary wherever the nontrivial Hamiltonian connects with a region of trivial Hamiltonian. The trajectories depicted in Figure 8 may not be smoothly connected to one another via a diffeomorphism, so, in order to connect two regions with differing topologies, the system's **h** vector must pass through the origin, closing the gap and hosting a zero energy mode. For these reasons, the above list of Majorana properties apply to the Abrikosov vortices made by applying a magnetic field to a type II SC as well. The locally destroyed SC state is a topological boundary in addition to the physical edges of the SC system.

2.4 Majorana Fermion

Experimentally, efforts to realize these so called Majorana zero energy modes or fermi level bogolons are ongoing, and, so far, several architectures have been proposed as a stage to host SC Majorana. In the previous section, it was noted that they may exist precisely in locations where the SC gap closes, or, equivalently, on the topological boundaries of the system. For simplicity, the first realization is found at the physical boundary.

The chiral Majorana fermion located on the system's edge, see Figure 11, is more difficult to manipulate than others discussed in this section, but there are papers

documenting successful braids of these edge states [20][21]. They have been observed on the phase boundary of a composite system formed by joining quantum anomolous Hall insulators (QAHI) and a topological superconductor (TSC). As their names imply, these modes only move in one direction and exist on the skin deep, 2D boundary of the system in four locations. In these types of experiments, the braiding of a certain

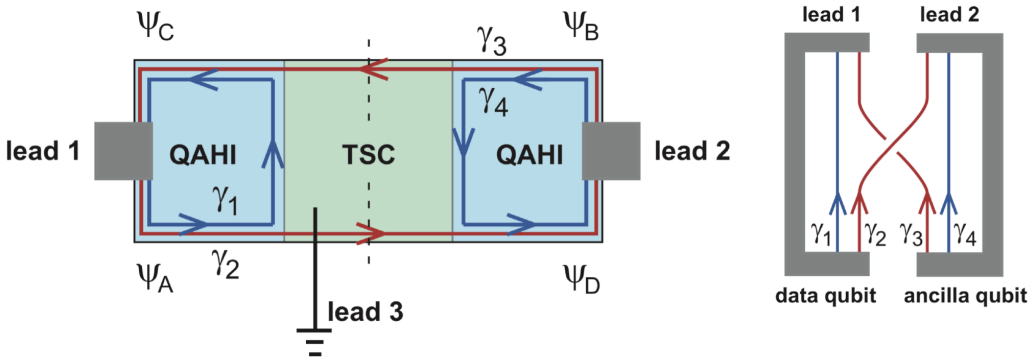

Figure 11: Chiral Majorana Fermion [21]. These chiral Majorana are found at the boundaries of the topological system where the SC gap must close in order to connect the topological region to the nontopological region. This system is comprised of a topological superconductor (TSC) and two quantum anomalous hall insulators (QAHI). The modes that run through the boundaries here are combined into fermionic operators, Ψ, which are then led through a "hardwired" braid which accomplishes a swapping of Majorana modes. However, in this scheme one may only swap γ_2 and γ_3 with not much freedom.

Majorana with another manifests as physically swapping leads as seen in Figure 11 on the right. This results in a braid operation, but it is an impractical implementation because there is no simple and quick method of braiding the other Majorana in the system. The braids are in a literal sense "hard wired" into the experiment since they are constrained to the geometrical layout of the material.

Another realization makes use of Josephson junctions placed on top of a topological insulator (TI), depicted in Figure 12. TI are another topological state of matter important to the discussion of Majorana, where deep within the bulk of a TI, the system is inert and will not allow supercurrent. However, on its surface, the TI

permits a skin deep SC state. Majorana appear at locations in between the SC islands where the local phase difference, $\Delta\phi$, is an odd multiple of π [22]. In contrast to the

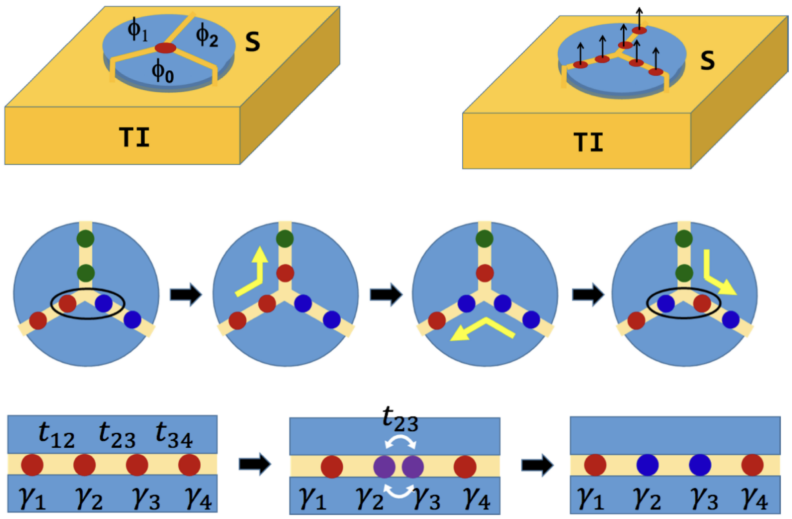

Figure 12: Joseph Junction Platform for Majorana Fermions [22]. Three Josephson junctions placed on top of a topological insulator with three different SC phases. At each point in between the islands where $\Delta\phi = \pi$, there exists a zero energy Majorana. These may be swapped in a 1D fashion where t is similar to the 1D kinetic energy hopping term from section 2.3

chiral Majorana which are 2D, these are 1D, existing only between the SC islands where t is the coupling parameter similar to the hopping potential introduced in the last section. Despite this, braids may be accomplished by adiabetically swapping these modes.

Yet another realization, which is the most promising, are the Majorana located within Abrikosov vortices created by magnetic fields where the SC gap locally closes in type II superconductors. In Figure 13 on the left, the setup for a successful attempt at trapping a Majorana is depicted. The s-wave, type II SC induces a 2D region of $p_x + ip_y$-wave state on the surface of the adhered TI, and a pin hole has been drilled through with radius, R, to sufficiently separate the ground state from higher energies. In the absence of such a pin hole, the first excited energy level is approximately $\frac{\Delta^2}{\epsilon_F}$ [23]. If one is to braid these vortices, the energy imparted by the braid interaction should

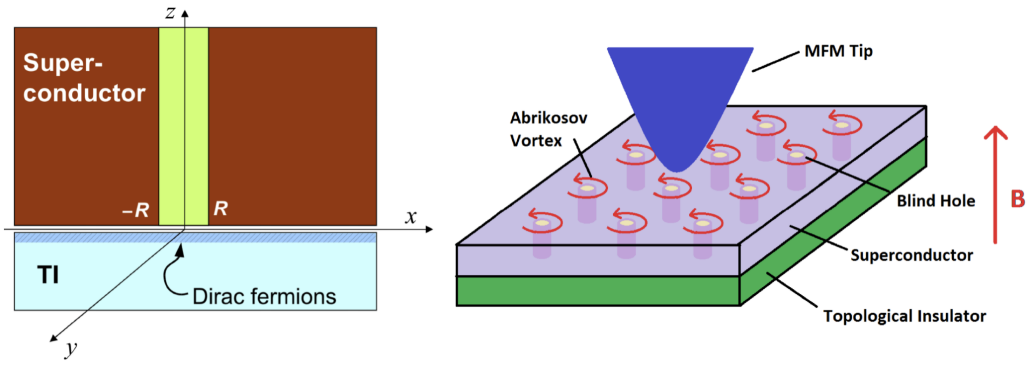

Figure 13: Pinned Majorana Vortex [23][24]. (Right) A type II, s-wave SC is placed on top of a TI to induce a $p_x + ip_y$-wave state. The ground state of this SC permits energy levels which are close enough to the ground state that adiabetic interaction would cause excitation to these levels. For this reason, a pin hole of radius R is drilled down to the TI which sufficiently separates the ground state from all higher energies. A magnetic field is then allowed to penetrate the system which induces a 2D Abrikosov vortex which hosts a Dirac fermion (Majorana). (Left) A crude topological quantum computer would utilize several pin sites with quasiparticle excitations in them. The Majorana in this system may be adiabetically exchanged with a multitude of tools (such as a Magnetic Force Microscope) generating braids.

not cause any excitations or else the process will fall apart. The 2D vortex at the bottom of the pin hole satisfies the Dirac/ Weyl equation (but the quasi particles here are spinless) and provides the ideal setting described in Section 2.2 for a Majorana zero energy mode. It has been shown that one may address each vortex individually with numerous experimental tools (e.g. magnetic force microscope [25], optical laser [26], scanning electron microscope [27], mechanical deformation [28]), with several demonstrations such as in Figure 14 where this group was capable of assembling them with extreme precision and sufficient speed, $\sim 10\frac{\mu m}{s}$ [26]. The ability to control each vortex allows scientists to braid vortices and the hosted Majorana found within each pin site as depicted on the right of Figure 13. Using this exact method, several groups have successfully produced Hadamard and CNOT gates, see Figure 15a and 15b [29][24][30].

To some degree, all options provided above set the stage for topological quantum

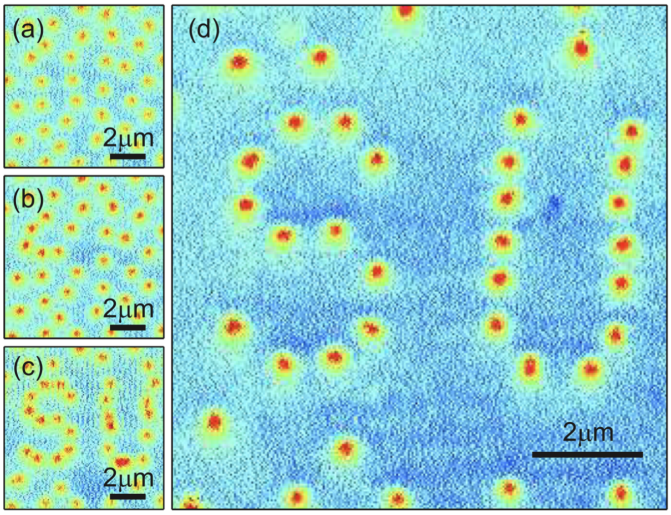

Figure 14: Magnetic Force Microscope Manipulation of SC Vortices [25].

computing, so, there are numerous methods of implementing a braiding operation on a set of Majorana modes. The particular realization is not as important here as the calculation of unitary operators which will be outlined in Chapter III in detail. However, to add some level of concreteness to the subsequent calculations, this document assumes the system in question is the same as depicted in Figure 13.

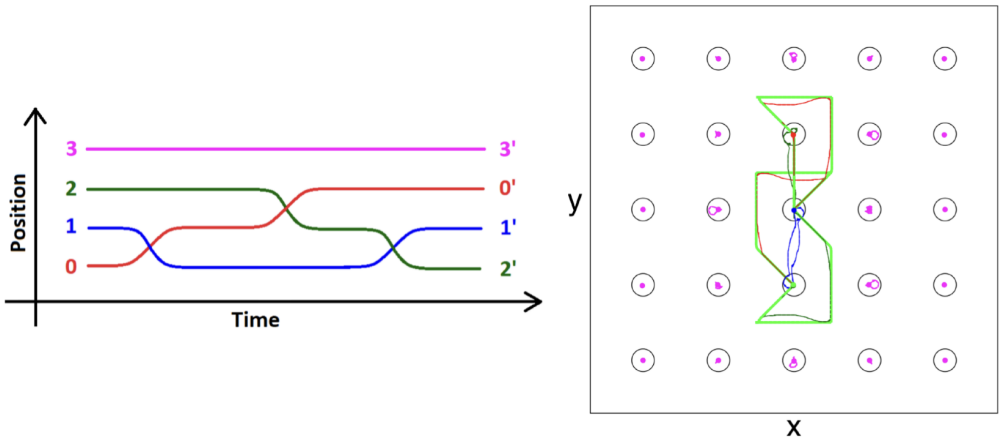

(a) Hadamard

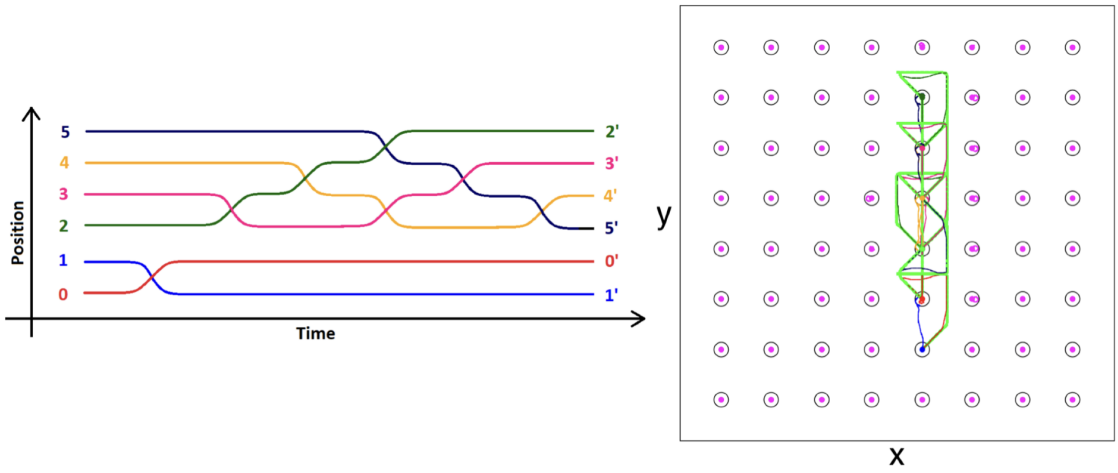

(b) CNOT

Figure 15: Majorana Braid for Hadamard and CNOT gates [24]. Each color coded line depicts the world line of a given Majorana mode. The actual motion of each vortex is depicted on the right where each circle is a pin site.

III. Quantum Gates

3.1 Setup

The setup for a primitive topological computer is pictorially depicted in Figure 16 where a SC region has been induced on the surface of a TI by an s-wave superconductor. A magnetic field penetrates the system at carved pin sites where the SC state is locally destroyed, closing the gap, and causing Abrikosov vortices to form surrounding the region of normal state. Because of gap closure in these locations, they are considered to be the topological boundaries and contain zero energy modes which are their own antiparticle.

These vortices may be moved about the region via several methods mentioned previously (magnetic force microscope, optical laser, etc.), and, so long as this is done *adiabatically*, the system will remain in one of the eigenstates of the ground state manifold, and the computer will be topologically protected.

Since the temporal phase change of a quantum state is dependent on the action integral, by varying the other parameters in the Hamiltonian, one discovers another phase contribution which is time independent. This *Berry phase* appears by variation of the physical locations of the Majorana modes in the Hamiltonian from Section 2.3. As one vortex is brought around another, the path taken generates a total phase change of π to the Majorana state which is represented in Figure 16 as *branch cuts* made starting at each vortex and ending somewhere on the borders of the region [24]. These cuts are made arbitrarily and will not affect the total calculation as long as everything is consistent. Since one may only interact with these vortices through some macroscopic means, the only actions one may take in regards to the majorana operators, γ_i, are,

i. *Relabelling:* $\gamma_i \to \gamma_j$

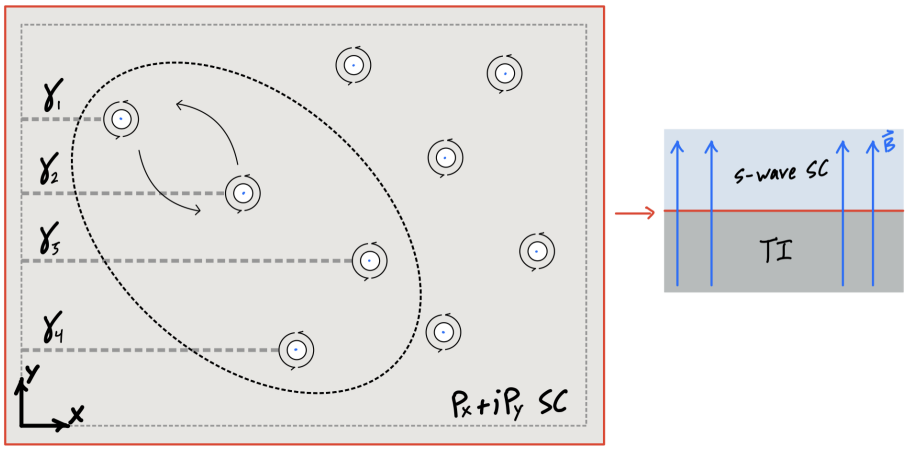

Figure 16: Majorana Fermion Setup. The system is located in a 2D $p_x + ip_y$- wave SC which is induced in a TI from an s-wave SC adjacent to the system. The computational states are defined using a collection of Majorana fermions located within the dotted oval. Vortices are made by allowing a magnetic field to penetrate the system. Braids are made by switching positions of the vortices where one must cross the arbitrary branch cuts.

ii. *Crossing branch cuts:* $\gamma_i \to -\gamma_j$

which may be accomplished by a physical exchange of Majorana.

Exchanging indistinguishable particles in 2D is qualitatively different than exchanging in 3D. This distinction is made pictorially in Figure 17. In 3D, all paths that a particle could traverse are deformable back to the original setting, therefore the final state must be symmetric (or antisymmetric) up to a global U(1) transformation. However, in 2D, paths traversed in front and behind another particle are distinct, and no smooth deformation can be made which brings the system back to the original setting without "slicing" through the second particle [18][2]. In terms of groups, the exchanges possible in a 3D, n particle system are described by the permutation group, P_n, depicted in Figure 18. Distinguishable (macroscopic) particle permutations are tractable and may be deformed back to the identity permutation of performing no action on the system. However, indistinguishable (microscopic) particles have permutations that may only be deformed to the identity up to a phase factor. In 3D, this

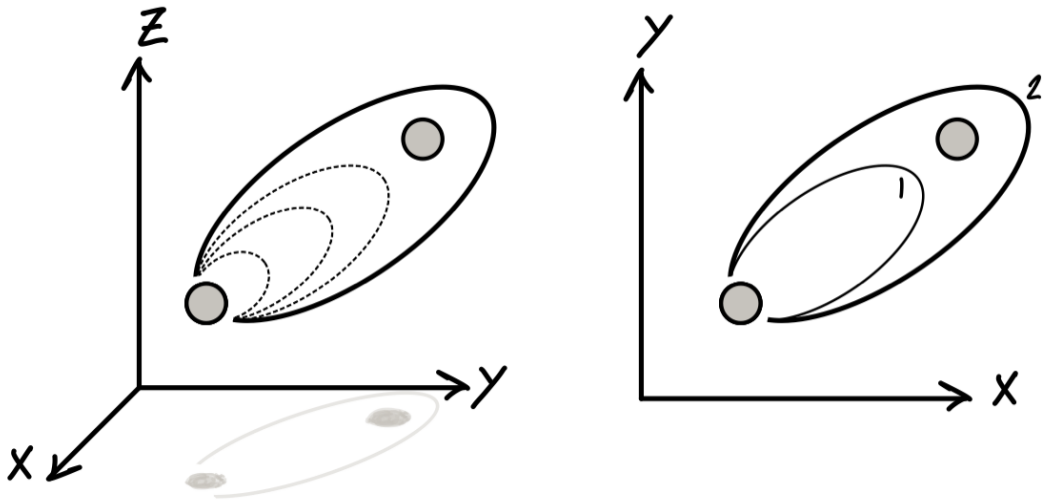

Figure 17: (Left) In three dimensions, the processes of moving an indistinguishable particle around another, results in a trajectory that may be continuously deformed beck to a single point. This means, after moving the particle around, the resulting state is only a U(1) phase difference of the original state, either symmetric or anti-symmetric. (Right) In two dimensions, the path cannot be deformed without slicing through the other particle. This means that the state resulting from moving the particle around and in front of are not the same, and path 2 does not result in a U(1) phase difference of the original state anymore.

phase factor may only be 0 or π which ensures that two exchanges return the state back to the original. However, the actions for 2D, n particles are more complicated. Because paths may not be freely deformed as in the 3D case, different trajectories result in different states. This behavior is described by the infinite braid group, B_n, instead. The braids here are formed from braiding the world lines of the vortices depicted in Figure 20.

By crossing branch cuts and braiding world lines, one only has access to the equivalence classes of braids, $B_n = \{[b_0], [b_1], [b_2], [b_3]...[b_{n-1}]\}$, where $[b]$ is represents all single braids that are deformable to one another. These classes of braids are depicted in Figure 19 and generate unitary rotations in the ground state manifold which do not commute. Therefore, the anyonic statistics of Majoranas are non-

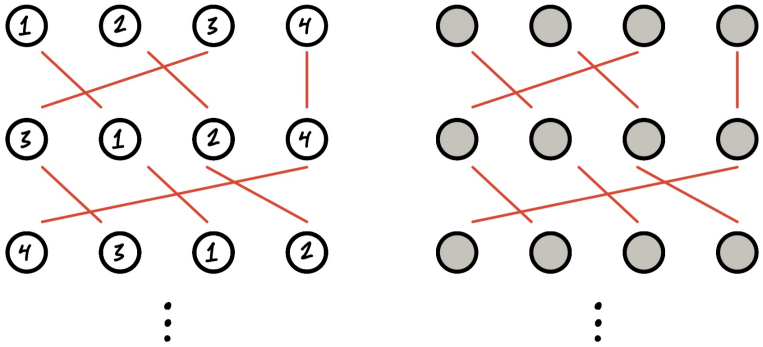

Figure 18: Permutation Group. The permutation group is a finite group. Here, P_4 is demonstrated for distinguishable particles and indistinguishable particles. On the left, since it is possible to tell the particles apart, it is possible to deform this group back to the identity. If the they are indistinguishable, the group cannot be deformed back to the identity.

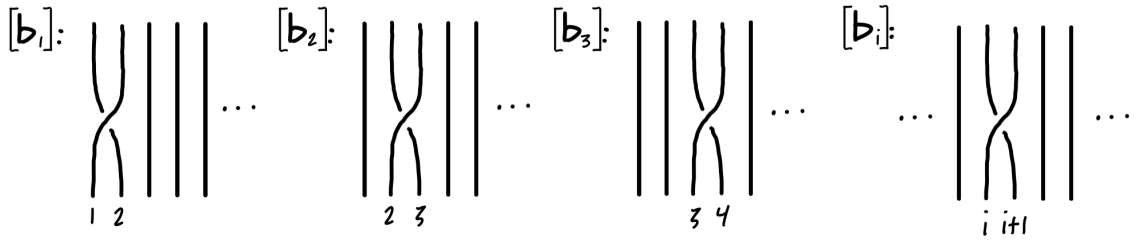

Figure 19: Braid Group. Unlike the permutation group which is finite, this group is an example of an infinite group. Each member of the group is some manner of twisting the strands over one another. It is easier to understand the infinite group in terms of equivalence classes which are displayed here where the members of each class may be deformed into one another.

abelian. The lack of accessibility of every member of the braid group is the exact reason that one may not form a universal gate operation from this formation. The nonabelian, anyonic statistics that arises naturally in this context has been detected [31][32][33].

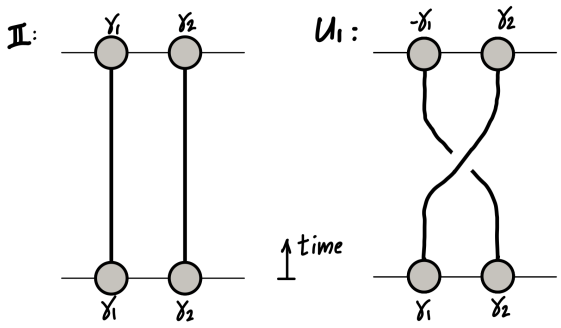

Figure 20: Unitary Transform. U_i as defined in this section represents a counterclockwise rotation of the world lines..

3.2 Calculation

The first step in this calculation is to define the ground state bogolon or Majorana operators,

$$\gamma_i = a^\dagger + a$$
$$\gamma_{i+1} = i(a^\dagger - a),$$

where each pair of γs can be associated with a, a highly non-local fermionic operator [33]. However, this a operator carries a slightly different meaning than those defined in Section 2.3. In a laboratory, when one is ready to take a measurement of this system, bringing the Majorana vortices together raises the degeneracy in the ground state. When this occurs, the resulting energy eigenstates are situated above the fermi surface. The occupation number associated with this operator represents the number of quasi-electrons populating the final upper energy state once a fusion is made between the two Majorana [2]. The computational states $|0\rangle$ and $|1\rangle$ are defined using this occupation number.

Now, one establishes the algebra associated with the creation and annihilation

operators,

$$\{a_1, a_1^\dagger\} = 1 \tag{4}$$

$$\{a_1, a_1\} = \{a_1^\dagger, a_1^\dagger\} = 0. \tag{5}$$

These relationships are motivated by Pauli exclusion, i.e. $(a_1^\dagger)^2 |0\rangle = 0$ and $(a_1 a_1^\dagger + a_1^\dagger a_1) |0\rangle = |0\rangle$. The Majorana operators then inherit their commutation relationship from Equation (4) and Equation (5) [33],

$$\{\gamma_i, \gamma_j\} = 2\delta_{i,j}. \tag{6}$$

This yields two rules for Majorana operators:

i. *Two identical γ operators in a row will annihilate to 1.*

ii. *Exchanging any two adjacent operators produces a negative sign.*

The representation that maps the braid group to a linear representation, $\rho : B_n \to \mathcal{LO}$, is an exponentiation of the operators [33][2][24],

$$\rho([b_i]) = U_i = e^{\frac{\pi}{4}\gamma_i\gamma_{i+1}} = \frac{1}{\sqrt{2}}(1 + \gamma_i\gamma_{i+1}), \tag{7}$$

see Appendix C for intermediate math and proof of unitarity.

To ensure this operator has the correct action on the Majorana, one performs a similarity transform on the γ operators,

$$\begin{aligned} U_i^\dagger \gamma_k U_i = \frac{1}{2}(1 + \gamma_{i+1}\gamma_i)\gamma_k(1 + \gamma_i\gamma_{i+1}) \\ = \frac{1}{2}\{\gamma_k + \gamma_k\gamma_i\gamma_{i+1} + \gamma_{i+1}\gamma_i\gamma_k + \gamma_{i+1}\gamma_i\gamma_k\gamma_i\gamma_{i+1}\}, \end{aligned}$$

where index k could be any Majorana including i and $i+1$. If $k \neq i$ or $i+1$, meaning

the transformation is on a Majorana operator uninvolved with the braid, then one would expect γ_k to be invariant under this transformation,

$$U_i^\dagger \gamma_k U_i = \frac{1}{2}\{\gamma_k + \gamma_k\gamma_i\gamma_{i+1} - \gamma_k\gamma_i\gamma_{i+1} + \gamma_k\gamma_{i+1}\gamma_i\gamma_i\gamma_{i+1}\} = \frac{1}{2}\{\gamma_k + \gamma_k\} = \gamma_k.$$

Commutation rules from Equation (6) are being used to move and cancel the operators throughout. If the transformation is being performed on operators that are involved in the braid,

$$\begin{aligned} U_i^\dagger \gamma_i U_i = \frac{1}{2}\{\gamma_i + \gamma_i\gamma_i\gamma_{i+1} + \gamma_{i+1}\gamma_i\gamma_i + \gamma_{i+1}\gamma_i\gamma_i\gamma_i\gamma_{i+1}\} \\ = \frac{1}{2}\{\gamma_i + \gamma_{i+1} + \gamma_{i+1} - \gamma_i\} = \gamma_{i+1}, \end{aligned}$$

and,

$$\begin{aligned} U_i^\dagger \gamma_{i+1} U_i = \frac{1}{2}\{\gamma_{i+1} + \gamma_{i+1}\gamma_i\gamma_{i+1} + \gamma_{i+1}\gamma_i\gamma_{i+1} + \gamma_{i+1}\gamma_i\gamma_{i+1}\gamma_i\gamma_{i+1}\} \\ = \frac{1}{2}\{\gamma_{i+1} - \gamma_i - \gamma_i - \gamma_{i+1}\} = -\gamma_i. \end{aligned}$$

These four transformations demonstrate that U_i does in fact represent a braid between Majorana i and $i+1$, two adjacent Majorana fermion. Since $\gamma_i \to \gamma_{i+1}$ and $\gamma_{i+1} \to -\gamma_i$, U_i represents a counterclockwise braid where γ_{i+1} crosses a branch cut as depicted in Section 3.1 Figure 20.

3.2.1 Two Majorana Fermions

Defining two adjacent Majorana in terms of fermionic operators

$$\begin{pmatrix} \gamma_1 \\ \gamma_2 \end{pmatrix} = \begin{pmatrix} 1 & 1 \\ -i & i \end{pmatrix} \begin{pmatrix} a_1 \\ a_1^\dagger \end{pmatrix}$$

and, by taking the inverse,

$$\begin{pmatrix} a_1 \\ a_1^\dagger \end{pmatrix} = \frac{1}{\sqrt{2}} \begin{pmatrix} 1 & i \\ 1 & -i \end{pmatrix} \begin{pmatrix} \gamma_1 \\ \gamma_2 \end{pmatrix}.$$

the fermionic operators may be solved in terms of Majorana. These form the computational basis, $\{|0\rangle, |1\rangle\} = \{|0\rangle, a_1^\dagger |0\rangle\}$. Next, simply operate on all members of the computational basis to determine the braid's effect on the ground state,

$$\begin{aligned} U_1^{(2)} |0\rangle &= \frac{1}{\sqrt{2}}(1 + \gamma_1\gamma_2) |0\rangle = \frac{1}{\sqrt{2}}(1 + i\{a_1^\dagger + a_1\}\{a_1^\dagger - a_1\}) |0\rangle \\ &= \frac{1}{\sqrt{2}}(1 + i\{a_1^\dagger a_1^\dagger - a_1^\dagger a_1 + a_1 a_1^\dagger - a_1 a_1\}) |0\rangle = \frac{1}{\sqrt{2}}(1+i) |0\rangle, \end{aligned}$$

and,

$$\begin{aligned} U_1^{(2)} |1\rangle &= \frac{1}{\sqrt{2}}(1 + i\{a_1^\dagger a_1^\dagger - a_1^\dagger a_1 + a_1 a_1^\dagger - a_1 a_1\}) |1\rangle \\ &= \frac{1}{\sqrt{2}}(1 + i\{-a_1^\dagger a_1 + a_1 a_1^\dagger\}) a_1^\dagger |0\rangle = \frac{1}{\sqrt{2}}(a_1^\dagger + i\{-a_1^\dagger a_1 a_1^\dagger + a_1 a_1^\dagger a_1^\dagger\}) |0\rangle \\ &= \frac{1}{\sqrt{2}}(a_1^\dagger - i a_1^\dagger\{1 - a_1^\dagger a_1\}) |0\rangle = \frac{1}{\sqrt{2}}(a_1^\dagger - i a_1^\dagger) |0\rangle = \frac{1}{\sqrt{2}}(1-i) |1\rangle, \end{aligned}$$

where Equation (4) and Equation (5) have been used [33]. Notice, the definition of the $|1\rangle$ state was used explicitly. Dividing out a global phase factor of $e^{i\frac{\pi}{4}}$, the counterclockwise braid of adjacent Majorana $U_1^{(2)}$ in matrix form is as follows,

$$U_1^{(2)} = \begin{pmatrix} 1 & 0 \\ 0 & i \end{pmatrix},$$

which is depicted in Figure 20. The number in the paranthesis superscript denotes the number of Majoranas in the system. To achieve the opposite directional braid, one

simply takes the complex conjugate. This braid operation is not useful at all because there is no coupling of states $|0\rangle$ and $|1\rangle$. To remedy this problem, the system requires two more Majorana.

3.2.2 Four Majorana Fermions

Now, with the addition of two more Majorana, one may form a new basis,

$$\{|00\rangle, |01\rangle, |10\rangle, |11\rangle\} = \{|0\rangle, a_2^\dagger|0\rangle, a_1^\dagger|0\rangle, a_1^\dagger a_2^\dagger|0\rangle\},$$

and Majorana operators [33],

$$\gamma_1 = a_1^\dagger + a_1$$
$$\gamma_2 = i(a_1^\dagger - a_1)$$
$$\gamma_3 = a_2^\dagger + a_2$$
$$\gamma_4 = i(a_2^\dagger - a_2).$$

The possible equivalence classes of braids in the B_4 group are depicted in Figure 21 with fermion definitions included as light and dark grey shading. Notice, $[b_1]$ (U_1) and

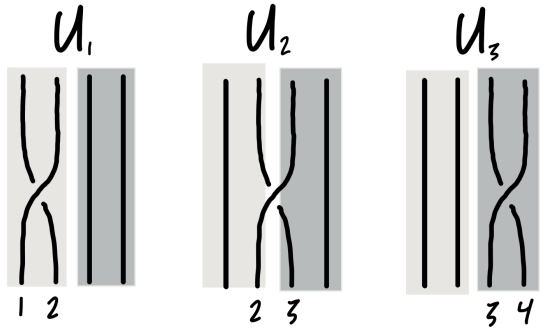

Figure 21: Four Majorana Braids. All braids available to a set of four strands of rope are encapsulated in this picture. Any possible combination of braids will be comprised of and deformed from some combination of the above braids. Light grey covers Majorana defined under fermion 1 while dark corresponds to fermion 2.

$[b_3]$ (U_3) involve Majorana defined under the same fermionic operator while $[b_2]$ (U_2) involve Majorana from different fermions. This observation provides the qualitative difference between the equivalence classes of a given braid group. With this setup, odd labelled braids will always be same fermion and even will always be different fermion braids.

Performing the identical operations from the single fermion case, U_1 and U_3 yield diagonalized matrices in the computational basis,

$$U_1^{(4)} = \begin{pmatrix} 1 & 0 & 0 & 0 \\ 0 & 1 & 0 & 0 \\ 0 & 0 & i & 0 \\ 0 & 0 & 0 & i \end{pmatrix}$$

and

$$U_3^{(4)} = \begin{pmatrix} 1 & 0 & 0 & 0 \\ 0 & i & 0 & 0 \\ 0 & 0 & 1 & 0 \\ 0 & 0 & 0 & i \end{pmatrix}.$$

These matrices are again diagonal with no coupling of states. However, when braiding Majorana fermions from two different fermionic operators, the transformation yields offdiagonal terms,

$$U_2^{(4)} = \frac{1}{\sqrt{2}} \begin{pmatrix} 1 & 0 & 0 & -i \\ 0 & 1 & -i & 0 \\ 0 & -i & 1 & 0 \\ -i & 0 & 0 & 1 \end{pmatrix},$$

which is the first case of state coupling.

The peculiar locations of non zero entries within $U_2^{(4)}$ are explained via parity, which, refers to the even or odd number of electrons in the superconducting bulk [17][18]. When two vortices are fused in the measurement process, the filling of the upper energy level may only happen by a single, unpaired electron. The numbers of electrons should remain unchanged throughout the braid, so the only states that may couple via braiding are those with same parity. For this reason, a state with even parity, $|11\rangle$ cannot become a state of odd parity, $|10\rangle$. The $U_2^{(4)}$ transformation above demonstrates this property as even states become coupled with even states and odd states become coupled odd states, i.e.

$$|00\rangle \longrightarrow \frac{1}{\sqrt{2}}(|00\rangle - i\,|11\rangle).$$

If one is to continue increasing dimensionality by adding more qubits, the result will be a sparsely populated matrix. This has very little use in computation because it is nowhere close to universal.

However, one may ameliorate the problem by working in either the even or odd computational subspaces [17][2]. This is done by redefining the computational states as $\left|\tilde{0}\right\rangle \equiv |00\rangle$ and $\left|\tilde{1}\right\rangle \equiv |11\rangle$, so that the transformations from above become,

$$\tilde{U}_1^{(4)} = \tilde{U}_3^{(4)} = \begin{array}{c} \begin{array}{cc} |00\rangle & |11\rangle \end{array} \\ \begin{pmatrix} 1 & 0 \\ 0 & i \end{pmatrix} \begin{array}{c} |00\rangle \\ |11\rangle \end{array} \end{array}$$

and,

$$\tilde{U}_2^{(4)} = \frac{1}{\sqrt{2}} \begin{array}{c} \begin{matrix} |00\rangle & |11\rangle \end{matrix} \\ \begin{pmatrix} 1 & -i \\ -i & 1 \end{pmatrix} \begin{matrix} |00\rangle \\ |11\rangle \end{matrix} \end{array}$$

For these reasons, instead of defining a single qubit from two Majorana, it is more practical to define a single qubit with all four Majorana.

It is worth noting again that the definition of each fermion is highly nonlocal and arbitrary. Instead of pairing adjacent vortices under one fermion, one may pair the center two and the outer two as in Figure 22. Physically, the braids $U_n^{(4)}$ are the

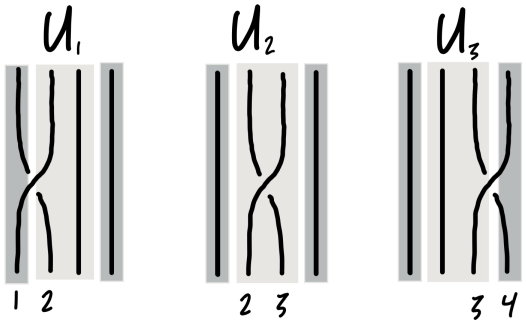

Figure 22: New Definition of Fermions. The definition of fermionic operators is arbitrary, and one may group Majorana in any combination. Here, the outer and inner Majorana are paired under a different fermion operator.

same as before, but the resulting matrices will initially seem different. However, upon closer inspection, this redefinition of fermions provide the same collection of gates. The new definition is equivalent to the previous definition with the only difference being swaps have been made between γ_2 and γ_3 and γ_3 and γ_4 prior to the moment of establishing this new definition. Therefore, nothing new is being done by exploring various definitions, and it is simpler to define Majorana adjacent to one another as a single fermion.

3.2.3 Six Majorana Fermions

Defining the basis here in a predictable fashion as in the previous two sections, i.e. $|111\rangle = a_1^\dagger a_2^\dagger a_3^\dagger |0\rangle$ or $|011\rangle = a_2^\dagger a_3^\dagger |0\rangle$, with three fermions and six Majoranas, the system now has five possible equivalence class braids.

The above calculations reveal a pattern regarding the trivial and coupling braids. When braiding two Majoranas from the same fermion, the diagonal matrix produced imparts a phase factor on the $|1\rangle$ state defined by that particular fermion operator. For example, when braiding γ_1 and γ_2 defined under a_1, the computational states $|1...\rangle$ recieve the phase factor i and states $|0...\rangle$ are unaffected. The ellipses in the above kets are meant to demonstrate that it is irrelevant how the other states are populated when using the U_1 braid. Similarly, the nontrivial coupling braids mix adjacent states in the ket. For example, the U_2 braid couples states $|00...\rangle$ and $|11...\rangle$, or $|01...\rangle$ and $|10...\rangle$ equivalently, with a phase factor of $-i$ placed off diagonal, where the remainder of the states could be anything.

Reducing dimensionality with qubit redefinition,

$$\begin{aligned}
\left|\tilde{0 0}\right\rangle &\equiv |\mathbf{00}0\rangle \\
\left|\tilde{0 1}\right\rangle &\equiv |\mathbf{01}1\rangle \\
\left|\tilde{1 0}\right\rangle &\equiv |\mathbf{10}1\rangle \\
\left|\tilde{1 1}\right\rangle &\equiv |\mathbf{11}0\rangle\,,
\end{aligned}$$

these intuitions make it easy to write out the matrices for the six Majorana case,

$$\tilde{U}_1^{(6)} = \begin{array}{c} \begin{array}{cccc} |000\rangle & |011\rangle & |101\rangle & |110\rangle \end{array} \\ \begin{pmatrix} 1 & 0 & 0 & 0 \\ 0 & 1 & 0 & 0 \\ 0 & 0 & i & 0 \\ 0 & 0 & 0 & i \end{pmatrix} \end{array} \begin{array}{l} |000\rangle \\ |011\rangle \\ |101\rangle \\ |110\rangle \end{array}$$

$$\tilde{U}_2^{(6)} = \frac{1}{\sqrt{2}} \begin{array}{c} \begin{array}{cccc} |000\rangle & |011\rangle & |101\rangle & |110\rangle \end{array} \\ \begin{pmatrix} 1 & 0 & 0 & -i \\ 0 & 1 & -i & 0 \\ 0 & -i & 1 & 0 \\ -i & 0 & 0 & 1 \end{pmatrix} \end{array} \begin{array}{l} |000\rangle \\ |011\rangle \\ |101\rangle \\ |110\rangle \end{array}$$

$$\tilde{U}_3^{(6)} = \begin{array}{c} \begin{array}{cccc} |000\rangle & |011\rangle & |101\rangle & |110\rangle \end{array} \\ \begin{pmatrix} 1 & 0 & 0 & 0 \\ 0 & i & 0 & 0 \\ 0 & 0 & 1 & 0 \\ 0 & 0 & 0 & i \end{pmatrix} \end{array} \begin{array}{l} |000\rangle \\ |011\rangle \\ |101\rangle \\ |110\rangle \end{array}$$

$$\tilde{U}_4^{(6)} = \frac{1}{\sqrt{2}} \begin{array}{c} \begin{matrix} |000\rangle & |011\rangle & |101\rangle & |110\rangle \end{matrix} \\ \begin{pmatrix} 1 & -i & 0 & 0 \\ -i & 1 & 0 & 0 \\ 0 & 0 & 1 & -i \\ 0 & 0 & -i & 1 \end{pmatrix} \end{array} \begin{matrix} |000\rangle \\ |011\rangle \\ |101\rangle \\ |110\rangle \end{matrix}$$

$$\tilde{U}_5^{(6)} = \begin{array}{c} \begin{matrix} |000\rangle & |011\rangle & |101\rangle & |110\rangle \end{matrix} \\ \begin{pmatrix} 1 & 0 & 0 & 0 \\ 0 & i & 0 & 0 \\ 0 & 0 & i & 0 \\ 0 & 0 & 0 & 1 \end{pmatrix} \end{array} \begin{matrix} |000\rangle \\ |011\rangle \\ |101\rangle \\ |110\rangle \end{matrix} .$$

3.2.4 Eight Majorana Fermions

Taking it one final step again with the addition of one more fermion and two more Majoranas. The computational states are defined in the predictable way. Here, the matrices are obviously so large that it is better to reduce to the even subspace

immediately. Showing the full matrices would not be beneficial.

$$\tilde{U}_1^{(8)} = \begin{pmatrix} 1 & 0 & 0 & 0 & 0 & 0 & 0 & 0 \\ 0 & 1 & 0 & 0 & 0 & 0 & 0 & 0 \\ 0 & 0 & 1 & 0 & 0 & 0 & 0 & 0 \\ 0 & 0 & 0 & 1 & 0 & 0 & 0 & 0 \\ 0 & 0 & 0 & 0 & i & 0 & 0 & 0 \\ 0 & 0 & 0 & 0 & 0 & i & 0 & 0 \\ 0 & 0 & 0 & 0 & 0 & 0 & i & 0 \\ 0 & 0 & 0 & 0 & 0 & 0 & 0 & i \end{pmatrix}$$

$$\tilde{U}_2^{(8)} = \frac{1}{\sqrt{2}} \begin{pmatrix} 1 & 0 & 0 & 0 & 0 & 0 & -i & 0 \\ 0 & 1 & 0 & 0 & 0 & 0 & 0 & -i \\ 0 & 0 & 1 & 0 & -i & 0 & 0 & 0 \\ 0 & 0 & 0 & 1 & 0 & -i & 0 & 0 \\ 0 & 0 & -i & 0 & 1 & 0 & 0 & 0 \\ 0 & 0 & 0 & -i & 0 & 1 & 0 & 0 \\ -i & 0 & 0 & 0 & 0 & 0 & 1 & 0 \\ 0 & -i & 0 & 0 & 0 & 0 & 0 & 1 \end{pmatrix}$$

$$\tilde{U}_3^{(8)} = \begin{pmatrix} 1 & 0 & 0 & 0 & 0 & 0 & 0 & 0 \\ 0 & 1 & 0 & 0 & 0 & 0 & 0 & 0 \\ 0 & 0 & i & 0 & 0 & 0 & 0 & 0 \\ 0 & 0 & 0 & i & 0 & 0 & 0 & 0 \\ 0 & 0 & 0 & 0 & 1 & 0 & 0 & 0 \\ 0 & 0 & 0 & 0 & 0 & 1 & 0 & 0 \\ 0 & 0 & 0 & 0 & 0 & 0 & i & 0 \\ 0 & 0 & 0 & 0 & 0 & 0 & 0 & i \end{pmatrix}$$

$$\tilde{U}_4^{(8)} = \frac{1}{\sqrt{2}} \begin{pmatrix} 1 & 0 & 0 & -i & 0 & 0 & 0 & 0 \\ 0 & 1 & -i & 0 & 0 & 0 & 0 & 0 \\ 0 & -i & 1 & 0 & 0 & 0 & 0 & 0 \\ -i & 0 & 0 & 1 & 0 & 0 & 0 & 0 \\ 0 & 0 & 0 & 0 & 1 & 0 & 0 & -i \\ 0 & 0 & 0 & 0 & 0 & 1 & -i & 0 \\ 0 & 0 & 0 & 0 & 0 & -i & 1 & 0 \\ 0 & 0 & 0 & 0 & -i & 0 & 0 & 1 \end{pmatrix}$$

$$\tilde{U}_5^{(8)} = \begin{pmatrix} 1 & 0 & 0 & 0 & 0 & 0 & 0 & 0 \\ 0 & i & 0 & 0 & 0 & 0 & 0 & 0 \\ 0 & 0 & 1 & 0 & 0 & 0 & 0 & 0 \\ 0 & 0 & 0 & i & 0 & 0 & 0 & 0 \\ 0 & 0 & 0 & 0 & 1 & 0 & 0 & 0 \\ 0 & 0 & 0 & 0 & 0 & i & 0 & 0 \\ 0 & 0 & 0 & 0 & 0 & 0 & 1 & 0 \\ 0 & 0 & 0 & 0 & 0 & 0 & 0 & i \end{pmatrix}$$

$$\tilde{U}_6^{(8)} = \begin{pmatrix} 1 & -i & 0 & 0 & 0 & 0 & 0 & 0 \\ -i & 1 & 0 & 0 & 0 & 0 & 0 & 0 \\ 0 & 0 & 1 & -i & 0 & 0 & 0 & 0 \\ 0 & 0 & -i & 1 & 0 & 0 & 0 & 0 \\ 0 & 0 & 0 & 0 & 1 & -i & 0 & 0 \\ 0 & 0 & 0 & 0 & -i & 1 & 0 & 0 \\ 0 & 0 & 0 & 0 & 0 & 0 & 1 & -i \\ 0 & 0 & 0 & 0 & 0 & 0 & -i & 1 \end{pmatrix}$$

$$\tilde{U}_7^{(8)} = \begin{pmatrix} 1 & 0 & 0 & 0 & 0 & 0 & 0 & 0 \\ 0 & i & 0 & 0 & 0 & 0 & 0 & 0 \\ 0 & 0 & i & 0 & 0 & 0 & 0 & 0 \\ 0 & 0 & 0 & 1 & 0 & 0 & 0 & 0 \\ 0 & 0 & 0 & 0 & i & 0 & 0 & 0 \\ 0 & 0 & 0 & 0 & 0 & 1 & 0 & 0 \\ 0 & 0 & 0 & 0 & 0 & 0 & 1 & 0 \\ 0 & 0 & 0 & 0 & 0 & 0 & 0 & i \end{pmatrix}$$

IV. Results and Analysis

4.1 General Discussion

As shown in the previous section, these definitions of qubits are extremely loose and somewhat difficult to describe. However, it is possible to collect some of the patterns that are visible when executing the above calculations. Firstly, each odd braid in the above construction yields a diagonal braid, while even yields a coupling braid, demonstrating that qubits will not entangle unless one shares a Majorana with another.

Immediately recognizeable from the above calculations is that the diagonal braids are directly related to the well known phase gate. For example, when attempting to be frugal and assigning two Majorana fermions to a single qubit, the phase gate appears naturally as the only braid possible,

$$U_1^{(2)} = \mathbf{S} = \begin{pmatrix} 1 & 0 \\ 0 & i \end{pmatrix}.$$

In fact, before reducing to a subspace, no matter how many Majorana are used in the computer, braiding any two defined under the same fermionic operator has the effect of applying the phase gate to the associated qubit. Once the space is then reduced to the even or odd subspace, the qubits fully represented in the reduction process still receive the phase gate tensor product formation upon braiding; however, braids for the qubit that has been partially left out, i.e. the final digit in the ket $|00...\mathbf{0}\rangle$, will now form a patterned tensor sum beginning with the phase gate. In other words, as depicted in figure 23, the final qubit is an ancillary qubit, and the final two braids involving this qubit will produce braids that break out of the pattern.

However, this pattern is not immediately apparent in the four Majorana case

because $\tilde{U}_1^{(4)}$ and $\tilde{U}_3^{(4)}$ appear to be identical. The six Majorana case does show this quality, where braiding Majorana from qubit one and two form the simple tensor product,

$$\tilde{U}_1^{(6)} = \mathbf{S} \otimes \mathbf{I}$$
$$\tilde{U}_3^{(6)} = \mathbf{I} \otimes \mathbf{S}.$$

The odd braid involves the ancillary qubit and results in the tensor sum of the phase

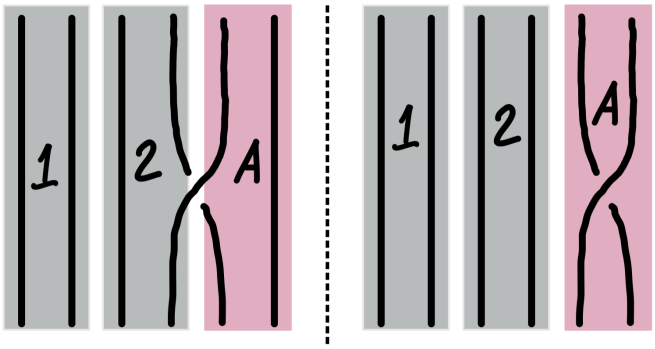

Figure 23: Ancillary Qubit. Each pair of Majorana are grouped to form a qubit. When reducing to the even or odd subspace, the ancillary qubit is partially left out of the final matrix transformation. Thus, the final two even or odd braids with this ancillary qubit will break the established pattern. Here, these two braids are depicted.

gate with its adjoint,

$$\tilde{U}_5^{(6)} = \mathbf{S} \oplus i\mathbf{S}^\dagger.$$

Similarly, the eight Majorana reduced case returns odd, trivial gates,

$$\tilde{U}_1^{(8)} = \mathbf{S} \otimes \mathbf{I} \otimes \mathbf{I}$$
$$\tilde{U}_3^{(8)} = \mathbf{I} \otimes \mathbf{S} \otimes \mathbf{I}$$
$$\tilde{U}_5^{(8)} = \mathbf{I} \otimes \mathbf{I} \otimes \mathbf{S}$$
$$\tilde{U}_7^{(8)} = \mathbf{S} \oplus i\mathbf{S}^\dagger \oplus i\mathbf{S}^\dagger \oplus \mathbf{S},$$

Without direct calculation, if one were to add another set of Majorana and reduce, the diagonal gates would continue this pattern,

$$\tilde{U}_1^{(10)} = \mathbf{S} \otimes \mathbf{I} \otimes \mathbf{I} \otimes \mathbf{I}$$

$$\tilde{U}_3^{(10)} = \mathbf{I} \otimes \mathbf{S} \otimes \mathbf{I} \otimes \mathbf{I}$$

$$\tilde{U}_5^{(10)} = \mathbf{I} \otimes \mathbf{I} \otimes \mathbf{S} \otimes \mathbf{I}$$

$$\tilde{U}_7^{(10)} = \mathbf{I} \otimes \mathbf{I} \otimes \mathbf{I} \otimes \mathbf{S}$$

$$\tilde{U}_9^{(10)} = \mathbf{S} \oplus i\mathbf{S}^\dagger \oplus i\mathbf{S}^\dagger \oplus \mathbf{S} \oplus i\mathbf{S}^\dagger \oplus \mathbf{S} \oplus \mathbf{S} \oplus i\mathbf{S}^\dagger.$$

As for the nontrivial, entanglement gates, the four Majorana gate, $\tilde{U}_2^{(4)}$, may be decomposed into the identity and Pauli $\mathbf{X}$ gate,

$$\tilde{U_2}^{(4)} = \frac{1}{\sqrt{2}} \begin{pmatrix} 1 & -i \\ -i & 1 \end{pmatrix} = \frac{1}{\sqrt{2}}(\mathbf{I} - i\mathbf{X}),$$

which is the Bloch sphere x-axis rotation operator,

$$R_x(\theta) = \cos\left(\frac{\theta}{2}\right)\mathbf{I} - i\sin\left(\frac{\theta}{2}\right)\mathbf{X},$$

evaluated for a specific, $\theta = \frac{\pi}{2}$. Therefore, when defining a qubit from four Majorana, this braid generates quarter rotations about the Bloch sphere's x-axis, and, in combination with the phase gate braids, it is only possible for these topological qubits to visit all six poles of the Bloch sphere as shown in Figure 24. Using this observation, one may create any of the quarter rotation Pauli $\mathbf{X}$, $\mathbf{Y}$, and $\mathbf{Z}$ gates as well, and, as an example, since the Hadamard gate places the state at the positive x-axis, it is automatically assumed that some combination of braid should place the qubit there as well. This corresponds to the third row qubit operation in Figure 24. This single

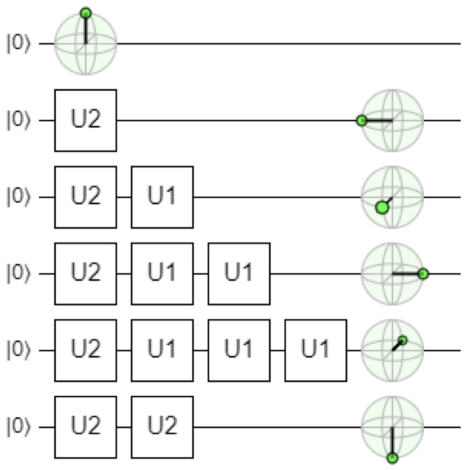

Figure 24: Quarter Rotation Pauli Spin Braids. A system of four Majorana fermions defining a single qubit has two braids one may create. These two braids only allow the state to visit the six poles of the Bloch sphere meaning the only gates available are quarter rotation Pauli **X**, **Y**, and **Z** gates. The third row in this image depicts a Hadamard gate and the final row depicts an **X** gate. This image was rendered using *https://algassert.com/quirk*.

qubit case highlights that the **X** gate emerges naturally in all native entangling gates.

This fact may be readily visualized in the six and eight Majorana gates, which may be decomposed into the identity and the aforementioned X gate,

$$\tilde{U}_2^{(6)} = \frac{1}{\sqrt{2}} \begin{pmatrix} 1 & 0 & 0 & -i \\ 0 & 1 & -i & 0 \\ 0 & -i & 1 & 0 \\ -i & 0 & 0 & 1 \end{pmatrix} = \frac{1}{\sqrt{2}} (\mathbf{I} \otimes \mathbf{I} - i\mathbf{X} \otimes \mathbf{X})$$

$$\tilde{U}_4^{(6)} = \frac{1}{\sqrt{2}} \begin{pmatrix} 1 & -i & 0 & 0 \\ -i & 1 & 0 & 0 \\ 0 & 0 & 1 & -i \\ 0 & 0 & -i & 1 \end{pmatrix} = \frac{1}{\sqrt{2}} (\mathbf{I} \otimes \mathbf{I} - i\mathbf{I} \otimes \mathbf{X})$$

$$\tilde{U}_2^{(8)} = \frac{1}{\sqrt{2}}(\mathbf{I}^{\otimes^3} - i\mathbf{X}\otimes\mathbf{X}\otimes\mathbf{I})$$
$$\tilde{U}_4^{(8)} = \frac{1}{\sqrt{2}}(\mathbf{I}^{\otimes^3} - i\mathbf{I}\otimes\mathbf{X}\otimes\mathbf{X})$$
$$\tilde{U}_6^{(8)} = \frac{1}{\sqrt{2}}(\mathbf{I}^{\otimes^3} - i\mathbf{I}\otimes\mathbf{I}\otimes\mathbf{X}).$$

In the above equations, a pattern may again be recognized. The $\mathbf{X}$ gate in the above decomposition are acting in pairs on qubits which share Majorana. The final braid couples the three qubit system with the ancillary qubit. This pattern will always occur in this fashion. For example, without additional work, adding two more Majorana would yield nontrivial entanglement braids,

$$\tilde{U}_2^{(10)} = \frac{1}{\sqrt{2}}(\mathbf{I}^{\otimes^4} - i\mathbf{X}\otimes\mathbf{X}\otimes\mathbf{I}\otimes\mathbf{I})$$
$$\tilde{U}_4^{(10)} = \frac{1}{\sqrt{2}}(\mathbf{I}^{\otimes^4} - i\mathbf{I}\otimes\mathbf{X}\otimes\mathbf{X}\otimes\mathbf{I})$$
$$\tilde{U}_6^{(10)} = \frac{1}{\sqrt{2}}(\mathbf{I}^{\otimes^4} - i\mathbf{I}\otimes\mathbf{I}\otimes\mathbf{X}\otimes\mathbf{X})$$
$$\tilde{U}_8^{(10)} = \frac{1}{\sqrt{2}}(\mathbf{I}^{\otimes^4} - i\mathbf{I}\otimes\mathbf{I}\otimes\mathbf{I}\otimes\mathbf{X}),$$

where the $\mathbf{X}^{\otimes^2}$ slides from left to right until the final even braid which breaks the pattern.

4.2 Steps Toward an Algorithm

With the intuitions gained from Chapter III, it is possible to partially outline a method of braid calculation from matrices. To begin, one must know how many Majorana fermions are needed to accomplish the desired quantum gate. As shown previously, parity dictates that the first useful set of gates comes from the even sub-

space of a four Majorana system. Even as the dimensionality of the system increases with additional qubits, one will always reduce to either the even or odd subspaces. When doing this, two of the Majorana from the group will become an ancillary qubit used to absorb topological charge [2]. Therefore, for an $n \times n$ quantum gate, one needs $n + 2$ Majoranas. For example, a 4×4 gate such as CNOT requires six Majorana fermions to implement.

Assuming adjacent Majorana are paired, with $n + 2$ Majorana fermions, there are $n + 1$ equivalence classes of braids accessible excluding their undo action. This collection of braids may be further divided into the $\frac{1}{2}n + 1$ odd diagonal gates and $\frac{1}{2}n$ even coupling gates. Using CNOT as an example again, with six Majorana, there are two even and three odd braids available.

These braids only allow the multi qubit state to visit the 6 poles of their individual Bloch spheres; no matter how they are entangled. Therefore, unitary gates that place the qubit state anywhere in between these poles has no representation as a braid, and they are not possible with this quantum computer. CNOT is the tensor sum of the identity and $\mathbf{X}$, so it is assumed here that such a gate has a braid representation.

Finally, for a system of $\frac{n}{2}$ qubits, $n + 2$ Majorana, and $n \times n$ gates, one may condense the patterns for the ith braid observed in the previous section into compact equations:

- For $i < n$ (Non-Ancillary Braids):
  - Odd Braids: $\tilde{U}_i^{(n+2)} = \mathbf{I}^{\otimes(i-1)} \otimes \mathbf{S} \otimes \mathbf{I}^{\otimes\frac{1}{2}(n-i-1)}$
  - Even Braids: $\tilde{U}_i^{(n+2)} = \frac{1}{\sqrt{2}}(\mathbf{I}^{\otimes\frac{n}{2}} - i\mathbf{I}^{\otimes(\frac{i}{2}-1)} \otimes \mathbf{X}^{\otimes 2} \otimes \mathbf{I}^{\otimes\frac{1}{2}(n-i-2)})$
- For $i \geq n$ (Ancillary Braids):
  - Final Odd Braid: $\tilde{U}_i^{(n+2)} = \tilde{U}_{i-2}^{(n)} \oplus i\tilde{U}_{i-2}^{(n)\dagger}$
  - Final Even Braid: $\tilde{U}_i^{(n+2)} = \frac{1}{\sqrt{2}}(\mathbf{I}^{\otimes\frac{n}{2}} - i\mathbf{I}^{\otimes(\frac{i}{2}-1)} \otimes \mathbf{X})$

4.3 Future Directions

The generator for braids is defined in equation 7 which has been provided in many papers. Phase contributions come from exponentiating the action integral resulting in two sources of phase contributions, temporal and parameter. The time independent Berry phase comes from varying parameters in the Hamiltonian. As seen in Section 2.3, the Hamiltonian takes the form,

$$H = -i\omega \sum \left[\xi_i \xi_{i+1}\right], \tag{8}$$

where only a subset of these ξs correspond to the zero energy modes, and ω is some constant related to kinetic energy. Therefore, the total phase would be,

$$\left|\Psi(t)\right\rangle = e^{-i\frac{t}{\hbar}H}\left|\Psi(0)\right\rangle = e^{-i\frac{t}{\hbar}(-i\omega)\sum[\xi_i\xi i+1]}\left|\Psi(0)\right\rangle = e^{-\frac{t\omega}{\hbar}\sum[\xi_i\xi_{i+1}]}\left|\Psi(0)\right\rangle. \tag{9}$$

Writing out the sum in the exponential,

$$\left|\Psi(t)\right\rangle = e^{-\frac{t\omega}{\hbar}[\xi_1\xi_2+\xi_2\xi_3+\xi_3\xi_4+\ldots]}\left|\Psi(0)\right\rangle. \tag{10}$$

So now, swapping the Majorana results in relabeling and placing a minus sign on the operators, therefore, the parameters that are being varied to impart a Berry phase are the operators in the Hamiltonian. For example, swapping actual Majorana modes on the edges of the system, γ_A and γ_B, and then pulling them out of the sum. The resulting exponential,

$$\left|\Psi(t)\right\rangle = e^{-\frac{t\omega}{\hbar}[\xi_2\xi_3+\xi_3\xi_4+\ldots]}e^{\frac{t\omega}{\hbar}\gamma_B\gamma_A}\left|\Psi(0)\right\rangle, \tag{11}$$

has this form where the minus signs cancel. The Berry phase is time independent, so set $t = t_0$ and group all of the constants together under some value, θ. The exponential is now,

$$|\Psi(t)\rangle = e^{\lambda} e^{\theta\gamma_2\gamma_1} |\Psi(0)\rangle , \tag{12}$$

where λ is all other parameters in the Hamiltonian held in place.

Previous papers have wanted to demonstrate clean results, so the constant in the exponential is set to $\frac{\pi}{4}$ to force the taylor expansion from Chapter III settle to a nice value. The generator for adjacent braids is therefore

$$e^{\frac{\pi}{4}\gamma_i\gamma_{i+1}}. \tag{13}$$

However, this value of θ is dependent on other parameters that are not immediately obvious. Since ξ in the original Hamiltonian is dependent on the kinetic energy and therefore also the momentum, one may input some reduced dimensional vector potential in the Hamiltonian, which augments the value of ξ in such a way that, as long as one remains in the adiabatic limit, this parameter provides an additional degree of freedom in the braiding operations. Written explicitly,

$$e^{\theta_b\gamma_i\gamma_{i+1}}, \tag{14}$$

where b is just a dummy parameter to indicate that we now have control over θ through the magnetic field. The taylor expansion to reveal this operators representation is identical to before except now it is left it in its more general form,

$$U_i = \cos\theta_b + \sin\theta_b\gamma_{i+1}\gamma_i. \tag{15}$$

This operator is unitary and has the same similarity transform on each γ. Now, the

linear operators for four Majoranas have the form,

$$\tilde{U_1} = \begin{pmatrix} \cos\theta_b + i\sin\theta_b & 0 \\ 0 & \cos\theta_b - i\sin\theta_b \end{pmatrix} = \begin{pmatrix} e^{i\theta_b} & 0 \\ 0 & e^{-i\theta_b} \end{pmatrix} \rightarrow \begin{pmatrix} 1 & 0 \\ 0 & e^{-2i\theta_b} \end{pmatrix}, \quad (16)$$

and

$$\tilde{U_2} = \begin{pmatrix} \cos\theta_b & -i\sin\theta_b \\ -i\sin\theta_b & \cos\theta_b \end{pmatrix} = \cos\theta_b \begin{pmatrix} 1 & 0 \\ 0 & 1 \end{pmatrix} - i\sin\theta_b \begin{pmatrix} 0 & 1 \\ 1 & 0 \end{pmatrix}, \quad (17)$$

V. Conclusions

Calculation of all possible linear representations of braids demonstrates that there are two classes of braids available. Braiding two Majorana defined under the same fermionic operator results in a diagonal, non-coupling rotation of the ground state manifold which imparts a phase difference of i between the two qubit states, and braids involving Majorana defined under different fermionic operators result in quantum gates that couple the same parity states in the ground state manifold with a phase difference of $-i$. If one is to pair adjacent Majorana under fermionic operators, the the trivial braids of non ancillary qubits are simply a tensor product of identity and phase gate operator where the phase gate is applied to the corresponding braided qubit. Coupling, non-ancillary braids result in tensor products of identity and $\mathbf{X}$ operators applied to the qubits that have traded Majorana. The final even and odd braids in the system involve the ancillary qubit which results in two operators that break from the above pattern. The final odd braid is a patterned tensor sum of phase gates, and the final even braid is similar to all other even braids except the $\mathbf{X}$ gate is applied to the final non-ancillary qubit singularly. These rotations only allow the qubits within the system to explore the 6 poles of the Bloch sphere. With these intuitions, one may now make guided determinations regarding calculating braids from unitary quantum gates. If the desired quantum gate causes any of the qubits to reach a state that is not in one of these six locations, it is clear that there does not exist a braid representation of this operator. If the opposite is true, then one may proceed with attempts at forming a braid. Because of parity, one requires $n+2$ Majoranas to represent $n \times n$ quantum gates, which have $\frac{1}{2}n+1$ trivial braids and $\frac{1}{2}n$ coupling braids.

Currently, quantum computers have the ability to perform actions that classical computers cannot, and, for this reason, the field is a growing even more rapidly with

many groups pushing what is possible. However, the state of the art systems that Google and IBM use for computation face the same scalability hurdle caused by decoherence. Thus, the search for fault tolerance in multi qubit systems is a necessary next step for the field of quantum information and quantum computation. The results in this document will allow scientists to possess some intuition when implementing an example of a fault tolerant quantum computing system. Of course, the above results are "less universal" than those implemented in a conventional system; however, as research into topological states of matter continues, a better system may be implemented with similar calculations and expanded qubit gates. These systems will hopefully provide the qubit of the 22_{nd} century.

Appendix A. Fourier Transform of 1D Continuous Chain

Using the fourier transform, $\mathcal{H}$ may be written as

$$\begin{aligned}\mathcal{H} = -\mu\{\frac{1}{N}\sum_{xkk'} e^{i(k-k')x}\}c_k^\dagger c_{k'} \\ - \frac{t}{2}\{\frac{1}{N}\sum_{xkk'} e^{i(k-k')x}\}e^{ik}c_k^\dagger c_{k'} - \frac{t}{2}\{\frac{1}{N}\sum_{xkk'} e^{i(k-k')x}\}e^{-ik'}c_k^\dagger c_{k'} \\ - \frac{\Delta e^{i\phi}}{2}\{\frac{1}{N}\sum_{xkk'} e^{-i(k+k')x}\}e^{-ik'}c_k c_{k'} - \frac{\Delta e^{-i\phi}}{2}\{\frac{1}{N}\sum_{xkk'} e^{i(k+k')x}\}e^{ik}c_k^\dagger c_{k'}^\dagger,\end{aligned}$$

and, after recognizing completion in the curly bracket terms,

$$\frac{1}{N}\sum_{xkk'} e^{i(k-k')x} = \delta_{kk'}, \tag{18}$$

we may simplify by setting $k = k'$ in the first two lines and $k' = -k$ in the latter two,

$$\mathcal{H} = -\mu\sum_k c_k^\dagger c_k - \frac{t}{2}\sum_k \left[e^{ik} + e^{-ik}\right] c_k^\dagger c_k - \frac{\Delta e^{i\phi}}{2}\sum_k e^{ik}c_k c_{-k} - \frac{\Delta e^{-i\phi}}{2}\sum_k e^{ik}c_k^\dagger c_{-k}^\dagger,$$

This pairing is exactly what is expected. Since this is a p-wave superconductor the pairs are of opposite momentum. Using $2\cos(k) = e^{ik} + e^{-ik}$ in the second term, this equation is further simplified to,

$$\mathcal{H} = \sum_k \{-\mu - t\cos(k)\}c_k^\dagger c_k - \frac{\Delta}{2}\sum_k e^{ik}\{e^{i\phi}c_k c_{-k} + e^{-i\phi}c_k^\dagger c_{-k}^\dagger\}. \tag{19}$$

Let $\epsilon_k \equiv -\mu - t\cos(k)$ and split the sums into the negative momentum values and

positive momentum values,

$$\mathcal{H} = \sum_{k>0} \epsilon_k c_k^\dagger c_k - \frac{\Delta}{2} \sum_{k>0} e^{ik} \{ e^{i\phi} c_k c_{-k} + e^{-i\phi} c_k^\dagger c_{-k}^\dagger \} + \sum_{k<0} \epsilon_k c_k^\dagger c_k - \frac{\Delta}{2} \sum_{k<0} e^{ik} \{ e^{i\phi} c_k c_{-k} + e^{-i\phi} c_k^\dagger c_{-k}^\dagger \}$$

Condense these sums by replacing k with -k on the bottom line,

$$\mathcal{H} = \sum_k \epsilon_k c_k^\dagger c_k - \frac{\Delta}{2} e^{ik} \{ e^{i\phi} c_k c_{-k} + e^{-i\phi} c_k^\dagger c_{-k}^\dagger \} + \epsilon_{-k} c_{-k}^\dagger c_{-k} - \frac{\Delta}{2} e^{-ik} \{ e^{i\phi} c_{-k} c_k + e^{-i\phi} c_{-k}^\dagger c_k^\dagger \}$$

we recognize that $\epsilon_k = \epsilon_{-k}$ because of the symmetric cosine term, and now using the anticommutation relationship between fermionic operators, $c_{-k} c_k = -c_k c_{-k}$, one may rewrite this equation and combine terms

$$\mathcal{H} = \sum_k \left[\epsilon_k c_k^\dagger c_k - \epsilon_k c_{-k} c_{-k}^\dagger + \frac{\Delta}{2} e^{i\phi} \{ e^{ik} - e^{-ik} \} c_{-k} c_k - \frac{\Delta}{2} e^{-i\phi} \{ e^{ik} - e^{-ik} \} c_k^\dagger c_{-k}^\dagger \right].$$

Then, recognizing $2i \sin(k) = e^{ik} - e^{-ik}$,

$$\mathcal{H} = \sum_k \left[\epsilon_k c_k^\dagger c_k - \epsilon_k c_{-k} c_{-k}^\dagger + i\Delta e^{i\phi} \sin(k) c_{-k} c_k - i\Delta e^{-i\phi} \sin(k) c_k^\dagger c_{-k}^\dagger \right].$$

Define $\Delta_k = i\Delta e^{i\phi} \sin(k)$, the Hamiltonian is finally,

$$\mathcal{H} = \sum_k \left[\epsilon_k c_k^\dagger c_k - \epsilon_k c_{-k} c_{-k}^\dagger + \Delta_k c_{-k} c_k + \Delta_k^* c_k^\dagger c_{-k}^\dagger \right].$$

Appendix B. Majorana Hamiltonian

Setting $\mu = 0$, $\Delta = t$, and $\phi = 0$, one may rewrite the Hamiltonian,

$$\mathcal{H} = \sum_{x=1}^{N} \left[-\mu c_x^\dagger c_x - \frac{t}{2} c_{x+1}^\dagger c_x - \frac{t}{2} c_x^\dagger c_{x+1} - \frac{1}{2}\Delta e^{i\phi} c_x c_{x+1} - \frac{1}{2}\Delta e^{-i\phi} c_{x+1}^\dagger c_x^\dagger \right],$$

as,

$$\mathcal{H} = -\frac{t}{2} \sum_{x=1}^{N} \left[c_{x+1}^\dagger c_x + c_x^\dagger c_{x+1} + c_x c_{x+1} + c_{x+1}^\dagger c_x^\dagger \right].$$

Now, splitting the c operators into real and imaginary components,

$$\mathcal{H} = -\frac{t}{8} \sum_{x=1}^{N} [\{\xi_{x+1,1} - i\xi_{x+1,2}\}\{\xi_{x,1} + i\xi_{x,2}\} + \{\xi_{x,1} - i\xi_{x,2}\}\{\xi_{x+1,1} + i\xi_{x+1,2}\} + \{\xi_{x,1} + i\xi_{x,2}\}\{\xi_{x+1,1} + i\xi_{x+1,2}\} + \{\xi_{x+1,1} - i\xi_{x+1,2}\}\{\xi_{x,1} - i\xi_{x,2}\}].$$

Expanding each term,

$$\begin{aligned} \mathcal{H} = -\frac{t}{8} \sum_{x=1}^{N} [& \xi_{x+1,1}\xi_{x,1} + i\xi_{x+1,1}\xi_{x,2} - i\xi_{x+1,2}\xi_{x,1} + \xi_{x+1,2}\xi_{x,2} + \\ & \xi_{x,1}\xi_{x+1,1} + i\xi_{x,1}\xi_{x+1,2} - i\xi_{x,2}\xi_{x+1,1} + \xi_{x,2}\xi_{x+1,2} + \\ & \xi_{x,1}\xi_{x+1,1} + i\xi_{x,1}\xi_{x+1,2} + i\xi_{x,2}\xi_{x+1,1} - \xi_{x,2}\xi_{x+1,2} + \\ & \xi_{x+1,1}\xi_{x,1} - i\xi_{x+1,1}\xi_{x,2} - i\xi_{x+1,2}\xi_{x,1} - \xi_{x+1,2}\xi_{x,2}], \end{aligned}$$

one may rearrange operators using the same commutation relationship for Majorana operators. This means that one may swap two different ξ operators at the cost of a

minus sign,

$$\begin{aligned}\mathcal{H} = -\frac{t}{8}\sum_{x=1}^{N}[&\xi_{x+1,1}\xi_{x,1} + i\xi_{x+1,1}\xi_{x,2} - i\xi_{x+1,2}\xi_{x,1} + \xi_{x+1,2}\xi_{x,2} \\ &-\xi_{x+1,1}\xi_{x,1} + i\xi_{x,1}\xi_{x+1,2} - i\xi_{x,2}\xi_{x+1,1} - \xi_{x+1,2}\xi_{x,2} + \\ &\xi_{x,1}\xi_{x+1,1} + i\xi_{x,1}\xi_{x+1,2} + i\xi_{x,2}\xi_{x+1,1} + \xi_{x+1,2}\xi_{x,2} \\ &-\xi_{x,1}\xi_{x+1,1} - i\xi_{x+1,1}\xi_{x,2} - i\xi_{x+1,2}\xi_{x,1} - \xi_{x+1,2}\xi_{x,2}].\end{aligned}$$

One may cancel all real terms since they have a negative counterpart,

$$\begin{aligned}\mathcal{H} = -\frac{ti}{8}\sum_{x=1}^{N}[&\xi_{x+1,1}\xi_{x,2} - \xi_{x+1,2}\xi_{x,1} + \xi_{x,1}\xi_{x+1,2} - \xi_{x,2}\xi_{x+1,1} \\ &+ \xi_{x,1}\xi_{x+1,2} + \xi_{x,2}\xi_{x+1,1} - \xi_{x+1,1}\xi_{x,2} - \xi_{x+1,2}\xi_{x,1}].\end{aligned}$$

Swapping the remaining operators, combining like terms and cancelling,

$$\mathcal{H} = -\frac{ti}{2}\sum_{x=1}^{N}[\xi_{x,1}\xi_{x+1,2}].$$

Appendix C. Braid Generator

Unitarity of the generator may be shown,

$$UU^\dagger = e^{\frac{\pi}{4}\gamma_i\gamma_{i+1}} e^{\frac{\pi}{4}\gamma_{i+1}\gamma_i} = e^{\frac{\pi}{4}(\gamma_i\gamma_{i+1}+\gamma_{i+1}\gamma_i)} = e^{\frac{\pi}{4}\{\gamma_i,\gamma_{i+1}\}} = e^{\frac{\pi}{4}(0)} = 1,$$

where the anticommutation relationship was used. To rewrite this operator in terms of a computational basis, Taylor expand the exponential,

$$\rho([b_i]) = e^{\frac{\pi}{4}\gamma_i\gamma_{i+1}} = 1+\frac{\pi}{4}\gamma_i\gamma_{i+1}+\frac{1}{2!}(\frac{\pi}{4}\gamma_i\gamma_{i+1})^2+\frac{1}{3!}(\frac{\pi}{4}\gamma_i\gamma_{i+1})^3+\frac{1}{4!}(\frac{\pi}{4}\gamma_i\gamma_{i+1})^4+... \quad (20)$$

Via commutation rules, we may swap two different Majorana mode operators at the cost of a minus sign and same operators annihilate one another. Therefore, all the even terms in eq. (20) may be rearranged and annihilated with one another since they come in pairs. The odd powers will almost do the same except they will always have a $\gamma_i\gamma_{i+1}$ left over. eq. (20) then becomes,

$$U_i = 1 + \frac{\pi}{4}\gamma_i\gamma_{i+1} - \frac{1}{2!}(\frac{\pi}{4})^2 + \frac{1}{3!}(\frac{\pi}{4})^3\gamma_i\gamma_{i+1} - \frac{1}{4!}(\frac{\pi}{4})^4 + ...$$

The terms with and without operators may be grouped like so,

$$U_i = \left[1 - \frac{1}{2!}(\frac{\pi}{4})^2 - \frac{1}{4!}(\frac{\pi}{4})^4 + ...\right] + \left[\frac{\pi}{4} + \frac{1}{3!}(\frac{\pi}{4})^3 + ...\right]\gamma_i\gamma_{i+1},$$

where it is obvious that these are the Taylor expansion of cosine and sine,

$$U_i = \cos(\frac{\pi}{4}) + \sin(\frac{\pi}{4})\gamma_i\gamma_{i+1} = \frac{1}{\sqrt{2}}(1 + \gamma_i\gamma_{i+1}).$$

Bibliography

1. Frank Arute, Kunal Arya, Ryan Babbush, Dave Bacon, Joseph C Bardin, Rami Barends, Rupak Biswas, Sergio Boixo, Fernando GSL Brandao, David A Buell, et al. Quantum supremacy using a programmable superconducting processor. *Nature*, 574(7779):505–510, 2019.

2. Chetan Nayak, Steven H Simon, Ady Stern, Michael Freedman, and Sankar Das Sarma. Non-abelian anyons and topological quantum computation. *Reviews of Modern Physics*, 80(3):1083, 2008.

3. David P. DiVincenzo. The physical implementation of quantum computation. *Fortschritte der Physik*, 48(9-11):771–783, Sep 2000.

4. Dénes Petz. Entropy, von neumann and the von neumann entropy. In *John von Neumann and the foundations of quantum physics*, pages 83–96. Springer, 2001.

5. Chetan Nayak, Steven H Simon, Ady Stern, Michael Freedman, and Sankar Das Sarma. Non-abelian anyons and topological quantum computation. *Reviews of Modern Physics*, 80(3):1083, 2008.

6. Wojciech H Zurek. Decoherence and the transition from quantum to classical-revisited. *Los Alamos Science*, 27:86–109, 2002.

7. A Yu Kitaev. Fault-tolerant quantum computation by anyons. *Annals of Physics*, 303(1):2–30, 2003.

8. Order parameters. `http://www.lassp.cornell.edu/sethna/OrderParameters/BrokenSymmetry.html`. Accessed: 2021-1-15.

9. Shou-cheng Zhang. Topological states of quantum matter. *Physics*, 1:6, 2008.

10. Physicists aim to classify all possible phases of matter. https://www.quantamagazine.org/physicists-aim-to-classify-all-possible-phases-of-matter-20180103/. Accessed: 2020-10-22.

11. Xiao-Gang Wen. Topological order: From long-range entangled quantum matter to a unified origin of light and electrons. *ISRN Condensed Matter Physics*, 2013, 2013.

12. Michael Levin and Xiao-Gang Wen. Detecting topological order in a ground state wave function. *Physical review letters*, 96(11):110405, 2006.

13. Xiao-Gang Wen. Topological orders in rigid states. *International Journal of Modern Physics B*, 4(02):239–271, 1990.

14. Helmut Eschrig. Theory of superconductivity a primer. 2001.

15. Hitoshi Murayama. Quantum field theory (a.k.a. second quantization), March 2005.

16. Joe Khachan and Stephen Bosi. Superconductivity, November 2010.

17. Martin Leijnse and Karsten Flensberg. Introduction to topological superconductivity and majorana fermions. *Semiconductor Science and Technology*, 27(12):124003, 2012.

18. Jason Alicea. New directions in the pursuit of majorana fermions in solid state systems. *Reports on progress in physics*, 75(7):076501, 2012.

19. A Yu Kitaev. Unpaired majorana fermions in quantum wires. *Physics-Uspekhi*, 44(10S):131–136, Oct 2001.

20. Yan-Feng Zhou, Zhe Hou, and Qing-Feng Sun. Non-abelian operation on chiral majorana fermions by quantum dots. *Physical Review B*, 99(19):195137, 2019.

21. Biao Lian, Xiao-Qi Sun, Abolhassan Vaezi, Xiao-Liang Qi, and Shou-Cheng Zhang. Non-abelian braiding of chiral majorana fermions. *arXiv preprint arXiv:1712.06156*, 2017.

22. Suraj S Hegde, Guang Yue, Yuxuan Wang, Erik Huemiller, DJ Van Harlingen, and Smitha Vishveshwara. A topological josephson junction platform for creating, manipulating, and braiding majorana bound states. *Annals of Physics*, page 168326, 2020.

23. AL Rakhmanov, AV Rozhkov, and Franco Nori. Majorana fermions in pinned vortices. *Physical Review B*, 84(7):075141, 2011.

24. Lachezar S. Georgiev. Topologically protected gates for quantum computation with non-abelian anyons in the pfaffian quantum hall state. *Physical Review B*, 74(23), Dec 2006.

25. Eric WJ Straver, Jennifer E Hoffman, Ophir M Auslaender, Daniel Rugar, and Kathryn A Moler. Controlled manipulation of individual vortices in a superconductor. *Applied Physics Letters*, 93(17):172514, 2008.

26. Ivan S Veshchunov, William Magrini, SV Mironov, AG Godin, J-B Trebbia, Alexandre I Buzdin, Ph Tamarat, and B Lounis. Optical manipulation of single flux quanta. *Nature communications*, 7:12801, 2016.

27. Jun-Yi Ge, Vladimir N Gladilin, Jacques Tempere, Cun Xue, Jozef T Devreese, Joris Van de Vondel, Youhe Zhou, and Victor V Moshchalkov. Nanoscale assembly of superconducting vortices with scanning tunnelling microscope tip. *Nature communications*, 7(1):1–7, 2016.

28. Anna Kremen, Shai Wissberg, Noam Haham, Eylon Persky, Yiftach Frenkel, and Beena Kalisky. Mechanical control of individual superconducting vortices. *Nano letters*, 16(3):1626–1630, 2016.

29. Daniel Litinski and Felix von Oppen. Braiding by majorana tracking and long-range cnot gates with color codes. *Phys. Rev. B*, 96:205413, Nov 2017.

30. X. Ma, C. J. O. Reichhardt, and C. Reichhardt. Braiding majorana fermions and creating quantum logic gates with vortices on a periodic pinning structure. *Phys. Rev. B*, 101:024514, Jan 2020.

31. Z-Y Xue. Detecting non-abelian statistics of majorana fermions in quantum nanowire networks. *JETP letters*, 94(3):213, 2011.

32. Jay D Sau, Sumanta Tewari, and S Das Sarma. Probing non-abelian statistics with majorana fermion interferometry in spin-orbit-coupled semiconductors. *Physical Review B*, 84(8):085109, 2011.

33. Dmitri A Ivanov. Non-abelian statistics of half-quantum vortices in p-wave superconductors. *Physical review letters*, 86(2):268, 2001.

REPORT DOCUMENTATION PAGE

Form Approved
OMB No. 0704–0188

1. REPORT DATE *(DD–MM–YYYY)*	2. REPORT TYPE	3. DATES COVERED *(From — To)*
25–03–2021	Master's Thesis	May 2020 — Mar 2021

4. TITLE AND SUBTITLE

Topological Realizations of Entangling Quantum Gates

5a. CONTRACT NUMBER

5b. GRANT NUMBER

5c. PROGRAM ELEMENT NUMBER

6. AUTHOR(S)

Scheppe, Adrian D, 2Lt, USAF

5d. PROJECT NUMBER

5e. TASK NUMBER

5f. WORK UNIT NUMBER

7. PERFORMING ORGANIZATION NAME(S) AND ADDRESS(ES)

Air Force Institute of Technology
Graduate School of Engineering and Management (AFIT/ENP)
2950 Hobson Way
WPAFB OH 45433-7765

8. PERFORMING ORGANIZATION REPORT NUMBER

AFIT-ENP-MS-21-M-134

9. SPONSORING / MONITORING AGENCY NAME(S) AND ADDRESS(ES)

Air Force Research Lab
26 Electronic Way
Rome Lab AFB NY 13441
COMM 315-330-2937
Email: laura.wessing@us.af.mil

10. SPONSOR/MONITOR'S ACRONYM(S)

AFRL/RITQ

11. SPONSOR/MONITOR'S REPORT NUMBER(S)

12. DISTRIBUTION / AVAILABILITY STATEMENT

DISTRIBUTION STATEMENT A:
APPROVED FOR PUBLIC RELEASE; DISTRIBUTION UNLIMITED.

13. SUPPLEMENTARY NOTES

14. ABSTRACT

Topological systems are immune to decoherence and provide a hunting ground for qubits that are fault tolerant. The process of calculating linear operator representations of Majorana fermion exchanges or braids is well known and well documented; however, there is no documented intuition or algorithm which provides the opposite; braids from quantum gates. In this document, all possible linear representations of single, double, triple, and quadruple qubit gates are calculated to find several key patterns which provide crucial insight into the manifestation of qubit gates. A $n \times n$ gate will require $n + 2$ Majoranas with $\frac{1}{2}n + 1$ trivial braids and $\frac{1}{2}n$ coupling braids possible. The native gates produced are either tensor products or tensor sums of the well known phase gate and Pauli $\mathbf{x}$ gate, demonstrating that a topological SC Majorana qubit may only explore the poles of the Bloch sphere. Additionally, the exact compact forms of all possible gates are listed. These insights are an important step to forming a complete understanding of the braids' effects on the multi qubit system which is necessary if one is to take advantage of this fault tolerant method of quantum computation.

15. SUBJECT TERMS

Quantum Computing, Topological States of Matter, Decoherence, Fault Tolerance, Quantum Gates

16. SECURITY CLASSIFICATION OF:			17. LIMITATION OF ABSTRACT	18. NUMBER OF PAGES	19a. NAME OF RESPONSIBLE PERSON
a. REPORT	b. ABSTRACT	c. THIS PAGE			Dr. Michael Pak, AFIT/ENP
U	U	U	UU	69	19b. TELEPHONE NUMBER *(include area code)* (937) 255-3636; michael.pak@afit.edu